

Manuscript Details

Manuscript number	GEOT_2019_130
Title	Travertine deposits constraining transfer zone neotectonic activity in geothermal areas: an example from the inner Northern Apennines (Bagno Vignoni-Val d'Orcia area, Italy)
Article type	Full Length Article

Abstract

Studying travertine deposits and the network of banded calcite veins that form their roots in the substratum can place important constraints on neotectonic activity and the seismotectonic settings of geothermal areas. In this paper, we present the results of integrated studies of a geothermal area located in the inner Northern Apennines (Bagno Vignoni area, Italy), where low magnitude ($M < 4$) seismicity suggests the occurrence of active faults, but information on their location, time-span of activity and seismotectonic setting is lacking. The study area is characterised by thermal springs ($T < 50^\circ\text{C}$) and travertine deposits well exposed in some saw-cut walls of abandoned quarries. We investigate the relationships between faults and the travertine deposits, in order to reconstruct the syn-sedimentary tectonic activity and the age of faulting, by combining analyses of: i) geological setting and structural/kinematic analyses of faults; ii) travertine morpho-structural and architectural setting; iii) travertine facies; iv) U-Th radiometric, stable- and clumped isotopes of travertine and banded calcite veins. The results highlight the occurrence of a wide brittle shear zone (> 3 km) formed by two orthogonal faults systems, NE- and NW-trending, characterised by oblique-slip to normal kinematics, respectively; these faults belong to a tract of the so-named "Grosseto-Pienza" transfer zone, crossing the southern Tuscany from the sea-coast to the outer Apennines belt. The Grosseto-Pienza transfer zone formed with extensional tectonics that have been affecting the inner Northern Apennines since the middle Miocene. U-Th dating of travertine and banded calcite veins indicates that faulting enhanced the hydrothermal fluid circulation since the middle Pleistocene, in a unvaried tectonic setting, as indicated by the $\delta^{18}\text{O}$ signature and temperature of the hydrothermal fluids, which remained stable through time. Faults activity continued until the Holocene and still produces seismicity. Finally, our findings permit to define the seismo-tectonic setting of this sector of the inner Northern Apennines, demonstrating more broadly the utility of travertine deposits in reconstructing the neotectonics in geothermal areas.

Keywords	Travertine; low-temperature geothermal areas; seismotectonic setting; tectonic activity; extensional tectonics; Northern Apennines
Taxonomy	Earth Sciences, Planetary Sciences
Manuscript category	Miscellaneous geothermal topics
Corresponding Author	Andrea Brogi
Corresponding Author's Institution	University of Bari
Order of Authors	Andrea Brogi, Domenico Liotta, Enrico Capezzuoli, Paola Matera, Sándor Kele, Michele Soligo, Paola Tuccimei, Giovanni Ruggieri, Tsai-Luen Yu, Chuan-Chou Shen, Katharine Huntington
Suggested reviewers	Koen Van Noten, Giancarlo Molli, Rudy Swennen, Mehmet Cihat Alcicek, Uğur TEMİZ

Submission Files Included in this PDF

File Name [File Type]

Dear Editor.docx [Cover Letter]

Transfer zone Bagno Vignoni travertine 9.docx [Manuscript File]

Fig. 1 - Schema appennino.jpg [Figure]

Fig. 2 - Carta con trasversali.jpg [Figure]

Fig. 3 - Carta Geologica.jpg [Figure]

Fig. 4 - Colonne stratigrafiche substrato.jpg [Figure]

Fig. 5 - Foto faglie.jpg [Figure]

Fig. 6 - panoramica travertini e dettagli.jpg [Figure]

Fig. 7 - Fissure ridge copy.jpg [Figure]

Fig. 8 - Fissure ridge anatomia.jpg [Figure]

Fig. 9 - facies copy.jpg [Figure]

Fig. 10 - travertine bodies and line drawing copy.jpg [Figure]

Fig. 11 - vene bandate cava 2 copy.jpg [Figure]

Fig. 12 - Vene bandate nel substrato.jpg [Figure]

Fig. 13 - vene bandate sez. sottile copy.jpg [Figure]

Fig. 14 - isotopi copy.jpg [Figure]

To view all the submission files, including those not included in the PDF, click on the manuscript title on your EVISE Homepage, then click 'Download zip file'.

Research Data Related to this Submission

There are no linked research data sets for this submission. The following reason is given:
Data will be made available on request

Dear Editor,

we would like to submit the manuscript entitled “Travertine deposits constraining transfer zone neotectonic activity in geothermal areas: an example from the inner Northern Apennines (Bagno Vignoni-Val d’Orcia area, Italy) to GEOTHERMICS for a possible publication.

This manuscript focuses on the relationships between faulting and hydrothermal fluid circulation in a low temperature geothermal area located in southern Tuscany, Italy, to the north of the Monte Amiata volcano-geothermal area. In particular, we constrain the role of transfer zones and seismicity in extensional settings for controlling the permeability maintenance of the structural conduits (i.e. faults) channelling Ca-bicarbonate rich fluids. We underline the role of the travertine deposits in reconstructing the tectonic activity through time, and in recording the geochemical features of the geothermal fluids flowing from thermal springs.

The methodology is based on the classical approach of the structural geology and field mapping, with integration of stratigraphic-sedimentological, geochemical (mainly stable and clumped isotopes on travertine) and geochronological (Th/U method) analyses.

We conclude that transfer zones play a fundamental role in controlling the location of thermal springs and therefore in channelling geothermal fluids from a reservoir up to the surface. In addition, through the analyses of the travertine deposits, we document, for the first time in the study area, a long-living tectonic activity and geothermal circulation, started since middle Pleistocene, at least.

Trusting you can find this work of interest for Geothermics,

With best regards, on behalf of the Authors

Andrea Brogi

University of Bari, Department of Earth and Geo-environmental Sciences
Via Orabona, 4 70125 BARI, Italy

andrea.brogi@uniba.it

1
2
3 Travertine deposits constraining transfer zone neotectonic activity
4 in geothermal areas: an example from the inner Northern Apennines
5 (Bagno Vignoni-Val d’Orcia area, Italy)
6
7
8
9

10 Andrea Brogi ^{a,b,*}, Domenico Liotta ^{a,b}, Enrico Capezzuoli ^c, Paola Matera ^a, Sándor Kele ^d,
11 Michele Soligo ^e, Paola Tuccimei ^e, Giovanni Ruggieri ^f, Tsai-Luen Yu ^{g,h}, Chuan-Chou Shen ^g,
12 Katharine W. Huntington ⁱ
13
14

15
16
17
18 ^a University of Bari, Department of Earth and Geoenvironmental Sciences, Via Orabona 4; Bari, Italy.

19 ^b IGG-CNR, Institute of Geosciences and Earth Resources; Via Moruzzi 1; Pisa, Italy

20 ^c University of Florence, Department of Earth Sciences, Via La Pira 4; Florence, Italy.

21 ^d Institute for Geological and Geochemical Research, Research Centre for Astronomy and Earth Sciences,
22 Hungarian Academy of Sciences, 1112 Budapest, Hungary.

23 ^e University of Rome3, Department of Science, Largo San L. Murialdo 1; Roma, Italy.

24 ^f IGG-CNR, Institute of Geosciences and Earth Resources; Via La Pira 4; Firenze, Italy

25 ^g High-Precision Mass Spectrometry and Environment Change Laboratory (HISPEC), Department of
26 Geosciences, National Taiwan University, Taipei 10617, Taiwan ROC

27 ^h Research Center for Future Earth, National Taiwan University, Taipei 10617, Taiwan ROC

28 ⁱ Department of Earth and Space Sciences, University of Washington, Seattle, WA 98195, USA
29
30
31
32

33 * Corresponding author: andrea.brogi@uniba.it
34
35
36

37 **Abstract**
38

39 Studying travertine deposits and the network of banded calcite veins that form their roots in the
40 substratum can place important constraints on neotectonic activity and the seismotectonic settings of
41 geothermal areas. In this paper, we present the results of integrated studies of a geothermal area located
42 in the inner Northern Apennines (Bagno Vignoni area, Italy), where low magnitude ($M < 4$) seismicity
43 suggests the occurrence of active faults, but information on their location, time-span of activity and
44 seismotectonic setting is lacking. The study area is characterised by thermal springs ($T < 50^\circ\text{C}$) and
45 travertine deposits well exposed in some saw-cut walls of abandoned quarries. We investigate the
46 relationships between faults and the travertine deposits, in order to reconstruct the syn-sedimentary
47 tectonic activity and the age of faulting, by combining analyses of: i) geological setting and
48 structural/kinematic analyses of faults; ii) travertine morpho-structural and architectural setting; iii)
49 travertine facies; iv) U-Th radiometric, stable- and clumped isotopes of travertine and banded calcite
50 veins. The results highlight the occurrence of a wide brittle shear zone (> 3 km) formed by two orthogonal
51 faults systems, NE- and NW-trending, characterised by oblique-slip to normal kinematics, respectively;
52 these faults belong to a tract of the so-named “Grosseto-Pienza” transfer zone, crossing the southern
53 Tuscany from the sea-coast to the outer Apennines belt. The Grosseto-Pienza transfer zone formed with
54
55
56
57
58
59
60

61
62 extensional tectonics that have been affecting the inner Northern Apennines since the middle Miocene. U-
63 Th dating of travertine and banded calcite veins indicates that faulting enhanced the hydrothermal fluid
64 circulation since the middle Pleistocene, in a unvaried tectonic setting, as indicated by the $\delta^{18}\text{O}$
65 signature and temperature of the hydrothermal fluids, which remained stable through time. Faults
66 activity continued until the Holocene and still produces seismicity. Finally, our findings permit to define
67 the seismo-tectonic setting of this sector of the inner Northern Apennines, demonstrating more broadly
68 the utility of travertine deposits in reconstructing the neotectonics in geothermal areas.
69
70
71

72
73
74 Key words: Travertine, low-temperature geothermal areas, seismotectonic setting, tectonic activity,
75 extensional tectonics
76
77

78 1. Introduction 79 80

81 Fault transfer zones consist of km-wide deformed crustal volumes, formed by parallel and/or
82 anastomosed fault segments that accommodate heterogeneous extension, splitting the thinned crust into
83 domains characterised by differentiated amount of extension (Gibbs, 1990). Transfer zones are therefore
84 wide brittle shear zones coexisting with near orthogonal normal faults, and contributing to produce
85 lithospheric and crustal thinning, as described for several regions affected by extensional tectonics in
86 continental crustal environments (Bally et al., 1981; Gibbs, 1990). In this framework, transfer zones result
87 as highly fractured rock-volumes where fluids can easily channeled (Lister et al., 1986; Ebinger, 1989;
88 Gibbs, 1990; Liotta, 1991; Rowland and Sibson, 2004; Alçiçek et al., 2013; Liotta et al. 2015), thus having a
89 role in controlling the emplacement of magmatic bodies in the upper crustal levels (Dini et al., 2008) and
90 in favouring the circulation of geothermal fluids (e.g. Rowland and Sibson, 2004).
91
92

93 The coexistence of normal and transfer fault zones has been documented in the inner Northern
94 Apennines, Italy, since at least the Neogene (Liotta, 1991; Carmignani et al., 1995; Liotta et al., 1998; Brogi
95 et al., 2005a; Brogi and Liotta, 2008; Barchi, 2010; Liotta et al. 2015), when magmatism and related
96 hydrothermal circulation were related to continuous (still ongoing) extensional processes, with a
97 prominent SW-NE-oriented distribution along the main transfer zones (Fig. 1). The present configuration
98 of the inner Northern Apennines (i.e. southern Tuscany and Northern Latium; Carmignani et al., 2001)
99 and northern Tyrrhenian sea (Bartole, 1995; Pascucci et al., 1999) derives from a rifting process that
100 thinned the lithosphere up to 30-50 km, (Calcagnile and Panza, 1981; Locardi and Nicolich, 1992) and the
101 crust up to 20-26 km (Di Stefano et al., 2011 with references therein), after the final thickening process
102 related to the Oligocene-early Miocene nappe stacking (Brunet et al., 2001; Molli, 2008; Bianco et al., 2015;
103 Rossetti et al., 2015).
104
105

106 In southern Tuscany, the NE-trending transfer zones were initially indicated as tectonic lineaments
107 (Fig. 1) since the early 1900s, by studies describing their geometric setting, geological features and
108 geomorphological evidences (Signorini, 1935; Merla, 1951; Ghelardoni, 1965; Bortolotti, 1966). However,
109 detailed field-based information on their architecture and kinematics is restricted to only a few areas
110 (Liotta, 1991; Pascucci et al., 2007; Brogi et al. 2013; 2014; Bianchi et al., 2015), where the role of the
111 structures associated to the transfer zones in controlling Neogene-Quaternary magmatism (Dini et al.,
112 2008; Acocella and Funiciello, 2006; Brogi et al., 2010a; Liotta et al., 2015) and seismicity (Mantovani et al.,
113 1995; Albarello et al., 2005; Viti et al., 2006; Brogi and Fabbrini, 2009; Viti et al., 2016) has been emphasized.
114
115
116
117
118
119
120

121
122 In the Amiata Mt (Fig. 1) volcano-geothermal area (Batini et al., 2003), NE-trending faults have been
123 considered as the main structures controlling the evolution of the middle Pleistocene volcano (Mazzuoli et
124 al., 1995; Ferrari et al., 1996; Cadoux and Pinti, 2009; Brogi, 2008a; Brogi et al., 2010a) and the development
125 of Hg-Sb ore deposits (Brogi et al., 2011). In a similar scenario, NE-trending structures were strictly
126 associated with the Pleistocene volcanism of the Northern Latium (Acocella and Funicello, 1999; 2006)
127 and magmatism in the northern Tyrrhenian Sea (Dini et al., 2008; Liotta et al., 2015).

128
129 Low-magnitude seismicity associated with these structures (Buonasorte et al., 1987; Liotta, 1991;
130 Brogi et al., 2014; Mantovani et al., 2015, Piccardi et al., 2017) suggests their tectonic activity, at least in
131 some tracts. This topic is extremely important as the seismotectonic setting of the inner Northern
132 Apennines is poorly defined, and scarce data are available to infer active and potentially dangerous faults.
133 Deeper knowledge of NE-trending structures is needed to better constrain their potential impact on the
134 seismicity of southern Tuscany, and role in controlling geothermal fluids circulation and storage at depth.

135
136 We address these issues by presenting an integrated method of study that includes sedimentological,
137 structural and geochemical approaches, focussing on the travertine deposits, as a marker of the fluid-rock
138 interaction through time; the study area is located in the sector of the inner Northern Apennines (Val
139 d'Orcia, Bagno Vignoni area), to the north of the Amiata Mt volcano-geothermal area (Fig. 2), where a
140 first-order NE-trending transfer zone (Grosseto-Pienza tectonic lineament in Bemporad et al., 1986) has
141 been documented since the 1980's (e.g., Bemporad et al., 1986), and where low-magnitude seismicity also
142 occurs (<http://cnt.rm.ingv.it/>). Thermal springs and widespread travertine deposits (active and fossil) are
143 aligned along this structure, indicating a strong relationship between faulting and fluid flow. Our study
144 deals to define: i) the geometrical and kinematics settings of faults; ii) the role of these structures in
145 channelling and controlling the fluid-rock interaction of the hydrothermal fluids flow through time; iii)
146 the age of faulting; iv) the role of faults in determining local seismicity.

147
148 The main results document a shear zone, at least 3 km wide, formed by NE-trending fault segments
149 that interrupt coeval NW-trending normal faults. The NE-trending faults controlled the location of the
150 thermal springs and the development of travertine deposits since the latest middle Pleistocene. Thermal
151 springs are still active and travertine is depositing in a slope system, thus suggesting that the activity of
152 the geothermal system is triggered by faulting, as also supported by the widespread low-magnitude
153 seismicity (e.g. seismic events occurred during March 2018; INGV: <http://cnt.rm.ingv.it/>).

154 155 156 157 158 159 160 161 2. Geologic setting

162
163 The Northern Apennines originated from the convergence and collision in the late Cretaceous–early
164 Miocene between the Adria promontory (of African plate pertinence) and the European plate, represented
165 by the Sardinia–Corsica massif (Molli, 2008, and references therein). This process gave rise to the stacking
166 of several tectonic units deriving from different palaeogeographic domains (Vai and Martini, 2001). From
167 the top, the units are (Carmignani et al., 1994): (a) the Ligurian Units, derived from the Ligurian-Piedmont
168 Domain, and consisting of remnants of Jurassic oceanic crust and its late Jurassic-Cretaceous, mainly
169 clayey, sedimentary cover; (b) the Sub-Ligurian Units (Sub-Ligurian Domain), made up of Cretaceous-
170 Oligocene turbidites; (c) the Tuscan Units forming a duplex system and composed of HP metamorphic
171 and sedimentary units ranging from Palaeozoic to Early Miocene in age (Pandeli et al., 1991; Carmignani
172 et al., 1994; Rossetti et al., 2002; Brogi and Giorgetti, 2010, 2012).

181
182 After nappe stacking, eastward migrating extension (e.g. Boccaletti et al., 1971; Lavecchia, 1988;
183 Patacca et al., 1990; Doglioni, 1991; Martini and Sagri, 1993; Carmignani et al., 1995; Liotta et al., 1998;
184 Molli, 2008; Barchi, 2010) affected the inner Northern Apennines (i.e., northern Tyrrhenian Sea and
185 Tuscany) from the early–middle Miocene to the Present (Jolivet et al., 1990; Storti, 1995; Carmignani et al.,
186 1995; Pascucci et al., 1999; Brunet et al., 2000). Although extension was a continuous process through time
187 (Brogi et al., 2005a, 2005b), two main stages can be described. The oldest extensional event occurred
188 during the Miocene (Carmignani et al., 1995; Dallmayer and Liotta, 1998; Liotta et al., 1998; Brogi and
189 Liotta, 2008; Brogi, 2011) and determined the development of mainly eastward dipping normal faults.
190 Fault development produced: (a) the lateral segmentation of the more competent levels within the
191 previously stacked tectonic units (Decandia et al., 1993); (b) the consequent westward rotation of their
192 hangingwalls and development of bowl-shaped tectonic depressions where Miocene continental to marine
193 sedimentation occurred (Brogi, 2004a; Brogi and Liotta, 2008); (c) the direct superimposition of the
194 Ligurian Units on the late Triassic evaporite and/or on the Palaeozoic phyllite, both representing regional
195 detachment levels (Dallmayer and Liotta, 1998; Brogi and Liotta, 2008); and (d) extension of at least 120%
196 (Carmignani et al., 1994; Brogi, 2006). The younger event (Dallmayer and Liotta, 1998; Barchi, 2010) has
197 been active since the Pliocene (Fig. 1). This phase of extension is characterized by NW-trending normal
198 faults crosscutting the previously developed structures (Calamai et al., 1970; Lazzarotto and Mazzanti,
199 1978; Mazzanti, 1966), and defining tectonic depressions where Pliocene-Quaternary marine to continental
200 sediments were deposited (Bossio et al., 1993; Martini and Sagri, 1993; Liotta, 1996; Brogi et al., 2013).
201 These depressions were coeval with NE-trending transfer zones (Liotta, 1991), along which magmatic
202 activity is concentrated (Acocella and Funicello, 2002, 2006; Dini et al., 2008; Brogi et al., 2010a; Liotta et
203 al., 2015). The amount of extension associated to this event is estimated to be about 6–7% (Carmignani et
204 al., 1994).

211 This extensional setting and evolution has been confirmed by many field and laboratory studies
212 (Lavecchia, 1988; Jolivet et al., 1990; Carmignani and Kligfield, 1990; Serri et al., 1993; Carmignani et al.,
213 1994, 1995; Liotta et al., 1998; Barchi, 2010; Barchi et al., 1998; Gualtieri et al., 1998; Negrodo et al., 1999;
214 Liotta and Ranalli, 1999; Rossetti et al., 1999; Brunet et al., 2000; Di Bucci and Mazzoli, 2002; Pera et al.,
215 2003; Pauselli et al., 2004; Lavecchia et al., 2004; Molli, 2008; Bartole, 1995; Pascucci et al., 1999; Collettini
216 et al., 2006; Dini et al., 2008; Brogi, 2008b). Alternative interpretations of the tectonic setting and evolution
217 have been proposed (Finetti et al., 2001; Finetti, 2006; Bonini and Moratti, 1995; Bonini and Sani, 2002;
218 Bonini et al., 2014), but an extensional framework better explains the tectonic setting of southern Tuscany
219 as discussed in many papers (e.g. Brogi et al., 2005a, 2005b; Brogi and Liotta, 2008; Brogi, 2011).

222 We focus our study on the Bagno Vignoni area (Figs 2 and 3), located along the transfer zone
223 named as “Grosseto-Pienza tectonic lineament”, affecting the western shoulder of the Neogene Siena-
224 Radicofani Basin (Fig. 2). This basin consists of a broad Neogene NNW–SSE oriented tectonic depression
225 where Pliocene marine sediments are unconformably overlain by Quaternary continental deposits (Bossio
226 et al., 1993; Liotta and Salvatorini, 1994; Pascucci et al., 2007).

229 In the basin shoulders, the Ligurian Units, Subligurian Units, and the Tuscan Nappe are widely
230 exposed (Fig. 2). Concerning the stratigraphic and tectonic setting of the Bagno Vignoni area, some
231 information were given by Losacco (1959) and more recently by Brogi et al. (2005c, 2007) who highlighted
232 duplex structures affecting the Tuscan Nappe, later delaminated during the extensional tectonics. A part
233 of the duplex system is exposed close to Bagno Vignoni locality (Fig. 3) while the remaining part has been
234 drilled (at least in part) by boreholes during exploration for thermal waters (Brogi et al., 2005c; 2007). The
235
236
237
238
239
240

241
242 duplex structure characterising the Tuscan Nappe reconstructed by boreholes and new fieldwork
243 (illustrated in the next paragraph) is illustrated in Fig. 4.
244
245

246 247 3. Methods 248

249
250 In order to (i) reconstruct the age, geometry and kinematics of faults and (ii) characterize the
251 geochemical features of the palaeofluids (i.e. stable isotopic composition and temperature), we carried
252 out integrated geological, geochemical and geochronological analyses in the area comprising the Bagno
253 Vignoni travertine deposits (Fig. 3).
254

255 First, we conducted new fieldwork focused on geologic mapping at 1:5.000 scale of an about 10 km²
256 (Fig. 3) area. The first aim of this work was to get information on the factors that controlled, and are still
257 controlling, the hydrothermal fluids flow and travertine deposition. Furthermore, in order to reconstruct
258 the interplay between tectonic activity and travertine deposition we have studied the travertine bodies, in
259 terms of: i) morpho-structural and architectural setting; ii) facies analyses; iii) structural and kinematic
260 setting. Furthermore, a geochemical study, in terms of stable and clumped isotopes, and U-Th dating have
261 been performed on the travertine deposits for better constrain the fluids provenience and age of
262 deposition (i.e. faulting).
263
264

265 Details of the methodologies concerning the stable and clumped isotopes analyses, and U-Th dating
266 are illustrated separately in the dedicated paragraphs.
267
268
269

270 4. Results of geological, geochemical and geochronological analysis 271

272
273 The following sections describe in different paragraphs our new observations of: i) the stratigraphic
274 features of the travertine substratum and structural setting of the area; ii) the architecture of the
275 travertine bodies; iii) stable- and clumped isotope analyses; and iv) geochronological analyses.
276
277
278

279 4.1 Stratigraphy of the travertine substratum **and** structural setting 280

281
282 We analysed the travertine substratum where it is exposed along the valley of the Orcia River (Fig.
283 3) that runs orthogonally with respect to the western margin of the Siena-Radicofani Basin. The
284 travertine substratum consists of: (i) late-Triassic-Oligocene sedimentary rocks belonging to the Tuscan
285 Nappe; (ii) Eocene-Oligocene carbonate-terrigenous succession belonging to the Subligurian Unit; (iii)
286 Cretaceous carbonate and terrigenous succession belonging to the external Ligurian Units (S.Fiora Unit);
287 and iv) Jurassic-Cretaceous ophiolite-bearing carbonate-terrigenous succession belonging to the inner
288 Ligurian Units (Ophiolitic Unit). Figure 4 summarizes the stratigraphic logs and the tectono/stratigraphic
289 relationships among the different units. All these units are unconformably overlain by Pliocene marine
290 sediments and, locally, by travertine deposits.
291
292

293 The pre-Neogene units experienced poliphased tectonic deformation during the Cretaceous-early
294 Miocene collisional and Neogene-Quaternary post-collisional evolution of the inner Northern Apennines.
295 Contractional structures (i.e. thrusts, reverse faults, folds and shear zones) affected the pre-Neogene Units
296 to form a tectonic pile (Fig. 4), partially exposed nearby the travertine quarries (Fig. 3), and mostly drilled
297
298
299
300

301
302 in the surroundings of the main active thermal springs (Brogi et al., 2007). Nevertheless, due to the effects
303 of the middle-late Miocene extensional tectonics, the Ligurian Units normally rest on the basal part of the
304 Tuscan succession (i.e. late Triassic evaporite), or on different units within the carbonate and terrigenous
305 succession (Fig. 3). Tectonic omissions within the Ligurian and Sub-Ligurian Units also occur frequently
306 within the whole study area (Fig. 3).
307

308
309 Pre-Neogene units and the Neogene-Quaternary deposits, as well as thrusts and extensional
310 detachments, are dissected by two high-angle fault systems (Fig. 3): (i) NE-trending faults, showing left-
311 lateral oblique-slip and normal movements, and (ii) NW-trending faults characterised by dominant
312 normal movements. NE-trending faults consist of anastomosed fault segments, up to 2 km long, that cross
313 the whole area forming an about 3 km wide shear zone: these are characterised by ~ten-meter offsets, and
314 gave rise to the narrow structural depression where the Orcia River developed (Fig. 3). At the
315 cartographic scale, NE-trending faults interrupt the lateral continuity of the NW-trending faults (Fig. 3)
316 and dissect both Neogene sediments and travertine deposits, highlighting that these structures were
317 active during the Neogene and Quaternary. The NW-trending faults display ten-meter offsets and
318 juxtapose Early Pliocene marine sediments with the Ligurian Units (Fig. 3). In contrast, in the
319 surroundings areas NW-trending faults are buried by late Pliocene sediments (cf. Liotta, 1994; Pascucci et
320 al., 2006; 2007; Brogi, 2011), suggesting that activity pre-dated the Early Pliocene.
321
322
323

324 Faults affecting the travertine substratum show offsets not exceeding 50 m (Fig. 3), and have core-
325 zones no larger than 5 m (Fig. 5a-e), consisting of brecciated and comminuted rocks (Fig. 5f). Well-
326 developed fractures, in some cases filled by calcite (Fig. 5), define the damage zones, in both the fault
327 walls (Fig. 5c-e). The fault slip-planes often contain mechanical striations and/or calcite/Fe-hydroxides
328 slickensides. Meso-faults affecting the Neogene deposits show displacements occasionally exceeding 10 m
329 (Fig. 5).
330

331 Structural and kinematic analyses were carried out on the carbonate and terrigenous succession of
332 the Tuscan Nappe (Figs 3 and 4), which is composed of the most favorable lithotypes to record striations.
333 More than 50 kinematic data were collected from 12 structural stations; the results are shown in the
334 diagrams of Fig. 3. Kinematic indicators of the NE-trending fault system show two superposed
335 movements, as reconstructed in few structural stations. The first one is defined by left-lateral oblique-slip
336 movements, while the second movement is characterized by a dominant vertical component (Fig. 5g).
337 Movements characterised by dominant normal components have also been recognized in the NW-
338 trending faults.
339
340
341

342 343 344 4.2 Travertine deposits

345
346 Travertine deposits have a maximum thickness of about 25 m and consist of two distinct bodies
347 located to the southwest and south of the Bagno Vignoni village (Fig. 3-6). The eastern body is still
348 growing in a restricted area (Fig. 6) where 50°C thermal water (Pentecost, 1994), drained from the thermal
349 spring feeding the “Bagno Grande” pool (Fig. 6d) is conveyed. In contrast, the western body is a fossil
350 deposit extensively quarried during the 1970’s (Fig. 6a). The three abandoned quarries are characterized
351 by saw-cut walls allowing the reconstruction of the internal architecture and different depositional events,
352 as well as the location of the feeder conduits of the palaeothermal springs. For this reason, we have
353 studied in detail the westernmost deposit.
354
355
356
357
358
359
360

361
362 In the following, we describe: i) architecture and lithofacies characterising the travertine body and its
363 depositional units; ii) the geometrical setting and textural features of the banded calcite veins; iii) the
364 results of stable- and clumped isotope analyses; iv) the geochronological analyses for age determination.
365
366
367

368 4.2.1 Architecture and lithofacies of the travertine deposit 369 370

371 On the top of the travertine deposits, NW- and NE-trending fissure ridges and cone-shape mounds
372 are aligned along the main faults (Fig. 6a), suggesting a structural control on their location. A NW-
373 trending fissure-ridge (Fissure ridge A, in Fig. 7), 56 m long, bounds the western slope of the Poggione hill
374 (Fig. 6a); the ridge is characterized by a central fissure ranging from 1 to 80 cm in width (Fig. 7). A few
375 tens of meters to the NW limit of the ridge, a cone-shape mound up to 50 cm high indicates the presence
376 of an isolated palaeothermal spring developed along the same fault that controlled the development of
377 fissure ridge A. Another fissure ridge, NW-trending and 60 m long (fissure ridge B, Fig. 7), occurs to the
378 south of the Poggione hill and delimits the eastern saw-cut wall of Quarry 2 (Figs 6 and 7). The geometry
379 of the bedded travertine is exposed in the westernmost wall of fissure ridge B along its entire length (at
380 least 80 m).
381
382
383

384 Decimeter-high cone-shape mounds are aligned along the south-eastern slope of the Poggione hill
385 (Fig. 6) for at least 100 m, revealing the geometry of the fault that fed the hydrothermal fluids from which
386 the eastern part of the travertine deposit originated. These mounds are partly dismantled but their
387 occurrence are indicated by up-ward cone-shape travertine beds.
388

389 Other minor fissure ridges characterise the whole travertine deposit (Fig. 6). Among these, fissure
390 ridge C (Fig. 6) is exposed in a small saw-cut wall showing the internal architecture of the ridge; our
391 observations show that it is characterized by several superposed lenticular/dome-shaped bedded
392 travertine bodies and corresponding to different depositional phases. The banded calcite vein
393 corresponding to the feeder conduit active during the latest travertine deposition is also recognizable (Fig.
394 8). This evidence indicates the shifting of the feeder fissure through time, therefore implying continuous
395 tectonic activity during travertine deposition.
396
397

398 The quarried travertine deposit (westernmost in Fig. 6a) corresponds to a slope depositional system
399 that passed to a distal zone characterised by sub-horizontal morphology and low-energy environment
400 (Fig. 9a); the whole deposit was fed by thermal springs developed on the NW- and NE trending fissure
401 ridges and mounds. In this scenario, laminated abiotic crystalline crusts, interrupted by small ponds of
402 microbial mats (Fig. 9b), formed where fluids run along slopes (cf Alçiçek et al., 2017), close to the paleo-
403 thermal springs. In the distal parts, fluids fed palustrine environments, where travertine deposited in
404 vegetated areas (Fig. 9c-d). The increasing amount of vegetation in the distal parts of the deposits
405 suggests the cooling and shifting of the flow system waters.
406
407

408 Travertine deposition was discontinuous through time, as highlighted by the numerous
409 unconformities that separate different depositional events, in some cases accompanied by paleosoils.
410 Nevertheless, the resulting travertine deposits can be estimated to be a maximum of about 25 m thick.
411

412 Four main lithofacies association (LF1-4 in Fig. 9), assembled in twelve main unconformity-bounded
413 stratigraphic units (S.U0-S.U11 in Fig. 10), have been categorised through the analyses of the quarries
414 saw-cuts:
415

- 416 1. Laminated porous microbialites (LF1), consisting of peloidal micritic layers locally with small
417 and very close pores (fenestral porosity) due to the presence of microbial mats and shrubs (Fig. 9c)
418
419
420

421
422 and/or layers with larger pores (mouldic porosity) due to the presence of paper-thin raft, bubbles,
423 puffy pastry-like structures and plant imprints (Fig. 9d). Their thickness varies from 0.5 cm to 10 cm.
424 Some units show high porous lens, 15 cm thick, mainly characterized by microbial mats and also karst
425 cavities partly filled by speleothems. Those kinds of deposits developed far from the slope, in lateral
426 flats and depressions where the water became colder than the source (Guo and Riding, 1999; Gandin
427 and Capezzuoli, 2014; Erthal et al., 2017).
428

429
430 2. Laminated abiotic crusts (LF2) composed by crystalline layers from 2 mm to 5 cm thick, with
431 variable dips ranging from more than 40° to 10°. The lamination is evident for color changes, from
432 white to yellow-rose-colored (Fig. 9b). Feather-like crystals make up the majority of layers and fan/ray
433 crystals are visible in some cases. Micro-terraces and small pools developed along slopes, in the flow
434 direction. Abiotic crust layers are locally interrupted by small microbial mats ponds, shrubs, microbial
435 lime and bubbles. Co-existence of abiotic crusts and micro-terraces are typical deposits of high-flux
436 regime that develop on slopes, close to the thermal springs.
437

438
439 3. Brecciated levels (LF3) made up of angular, cm-to-m-sized travertine clasts in a fine grey
440 carbonate matrix, without a preferential orientation (Fig. 9e). These deposits originated from
441 disrupted travertine beds in small muddy morphological depressions (Gradzinski et al., 2014) or as
442 possible earthquake-triggered soft-sediment deformation structures (seismites - Brogi et al., 2018).
443

444 4. Micritic lime deposit (LF4) composed by massive, fine-grained, grey-brownish-colored compact
445 limestone (Fig. 9e), developed in distal, palustrine environment characterized by cool and shallow
446 ponds (Gandin and Capezzuoli, 2014).
447

448
449 According to the classification of Capezzuoli et al. (2014), facies association exposed in the
450 quarried travertine deposit (westernmost in Fig. 6a) corresponds to a slope depositional system that
451 passes to a distal zone characterised by sub-horizontal morphology and low-energy environment (Fig.
452 9a); the whole deposit was fed by thermal springs developed on the NW- and NE trending fissure ridges
453 and mounds. In this scenario, laminated abiotic crystalline crusts, interrupted by small ponds of microbial
454 mats (Fig. 9b), formed where fluids run along slopes (cf Alçiçek et al., 2017), close to the palaeo-thermal
455 springs. In the distal parts, fluids fed palustrine environments, where travertine deposited in vegetated
456 areas (Fig. 9c-d). The increasing amount of plants in the distal parts of the deposits suggest the cooling
457 and shifting of the waters flow system.
458

459
460 In quarries 1 and 2 the lower travertine units (from S.U0 to S.U5) are exposed (Fig. 10a). These are
461 characterised by gently dipping beds mainly composed of LF1+LF3+LF4, indicating a dominant low-
462 energy depositional environment, at least as it concerns the S.U0-S.U3 levels. In Quarry 2, a well-
463 developed palaeosoil, up to 2 m thick, separating the S.U0 from the S.U1 is exposed in the northern saw-
464 cut wall (Fig. 10b). Its occurrence suggests a prolonged depositional stasis, accompanied by erosional
465 processes and pedogenesis, before the deposition of the S.U1 level.
466

467
468 Quarry 3 (Fig. 10) shows most of the travertine succession (from S.U2 to S.U 11). Succession from
469 S.U2 to S.U5 is mostly formed by distal (i.e. palustrine: F1+F3+F4) facies associations; in contrast, the
470 successions from S.U6 to S.U11 are mainly characterised by proximal (i.e. slope: F2) facies associations
471 developed close to the palaeo-thermal springs located along the fissure ridge B (Fig. 10). The easternmost
472 saw-cut wall shows five depositional units that formed on the western flank of the previously mentioned
473 fissure ridge.
474

475
476 The lower part of the travertine succession (S.U0-S.U3) was dissected by faults. In particular, the S.U0
477 was strongly dissected by NW-trending faults; deformation affected 10 meters of the S.U0 succession as
478

481
482 recognised in the western and eastern saw-cut walls of the Quarry 2 (Fig. 11a). Most of tectonic
483 deformation affected the S.U0 and was accompanied by fluid circulation that deposited banded calcite
484 veins in a time-period spanning at least 23.3 ± 0.6 and 9.5 ± 1.8 ka. Several parallel-banded calcite veins
485 cross-cutting each other developed within the fault zones (Fig. 11c-d). The fault zone was partially
486 eroded and buried under the S.U1 (Fig. 11a-d). Nevertheless, faulting continued after the deposition of
487 the S.U1, producing the cracking and tilting of bedded travertine blocks and the development of open
488 fractures, up to 1.5 m in width, filled by bedded travertine (Fig. 11a-b). Such a neoformal travertine
489 was later dissected; banded calcite veins developed along the fault zone therefore suggesting that faulting
490 was accompanied by hydrothermal fluid circulation up to 9.5 ± 1.8 ka (Fig. 11e).

491
492
493
494 Saw-cut walls of all quarries do not permit us to evaluate if such a fault also dissected the overlying
495 units, even if it is expected.
496
497

498 499 4.2.2 Geometric and textural features of the banded calcite veins 500

501 Most of the banded calcite veins are exposed in the saw-cut walls of the quarries, but in some cases
502 banded veins have also been recognised in the quarry-floors, where the substratum is exposed in
503 restricted windows (Fig. 12a-c). In other cases, banded calcite veins filled the central fissure of minor
504 fissure ridges or have been recognised crossing the travertine beds outside the quarries (Fig. 12d-e). In all
505 cases, the banded calcite veins are NW- and NE-trending, parallel to the main faults recognised in the
506 whole area (Fig. 10a). Veins cross-cut each-other and define volumes of deformed travertine beds with a
507 concentrated vein network. In some cases, the chronological relationships among veins are clear but in
508 other cases veins are mutually cross-cutting, defining very complex vein arrays.
509

510
511 Each vein consists of millimeter thick, parallel and/or subparallel vertical crystal bands with different
512 colours: white, grey, yellowish, red and more rarely brownish bands (Fig. 13). In some cases, light-
513 transparent bands have internal black/grey shades. The contact between veins and travertine is sharp.
514 Vein crystals grew normal to the wall-rock, toward the central part of fractures, thus forming
515 symmetrical, isopachous, or less frequent botryoidal mm-to-cm thick crusts (Fig. 13a). Banded veins are
516 commonly sealed although discontinuous voids rimmed by festoons can locally be observed in the central
517 part of the vein.
518

519
520 According to Capezzuoli et al. (2018), Type A bands with elongate-blocky calcite crystals,
521 characterized by 0.17 – 2.6 mm in length and wavy extinction, and Type B bands with microcrystalline
522 (microsparite-to micrite) calcite crystals have been recognised characterising most laminae (Fig. 13b).
523 The Type A elongate-blocky crystals seem to nucleate from Type B microcrystalline cone and grow
524 perpendicular to the vein wall.
525
526
527

528 529 4.2.3 Stable and clumped isotope analyses 530

531
532 $\delta^{13}\text{C}$ and $\delta^{18}\text{O}$ analyses have been made on eight key samples (Fig. 10a), some of which used also
533 for radiometric ages determination (Table 1). BV 12 and BV 16 are banded calcite veins from Quarry 2
534 (Fig. 11); BV 10 and BV 11 are respectively from the LF2 and banded calcite vein crossing the S.U1 in the
535 Quarry 2 (Fig. 11e); BV 15 is a LF2 crystalline crust bedded travertine collected SW to the Quarry 3; BGV
536 8 consists of a LF2 crystalline crust collected close to the previous sample. BGV 7 is a LF1 microbial mat
537
538
539
540

541 collected in the Quarry 3 and BV 13 is LF2 crystalline crust located in Quarry 2. See Figs 10a and 11 for
542 their location.
543
544

545 Stable carbon and oxygen isotope measurements were performed on powders at the Institute for
546 Geological and Geochemical Research, Hungarian Academy of Sciences, Budapest, Hungary, using the
547 continuous flow technique with the H₃PO₄ digestion method (Spötl and Vennemann, 2003). ¹³C/¹²C and
548 ¹⁸O/¹⁶O ratios of CO₂ generated by acid reaction were measured using a Thermo Finnigan Delta Plus XP
549 continuous flow mass spectrometer equipped with an automated GasBench II. The results are expressed
550 in the δ -notation [δ = (R1/R2 - 1) × 1000] where R1 is the ¹³C/¹²C or ¹⁸O/¹⁶O ratio of the sample and R2
551 is the corresponding ratio of the Vienna Pee Dee Belemnite (VPDB) standard, in parts per thousand.
552 Finnigan Delta Plus XP continuous flow mass mean values are given in the standard δ -notation in parts
553 per thousand (‰) relative to VPDB (δ ¹³C and δ ¹⁸O) and Vienna Standard Mean Ocean Water (VSMOW;
554 δ ¹⁸O). Duplicates of standards and samples reproduced values.
555
556

557 Results of the carbon and oxygen isotope compositions of all samples are reported in Table 2. δ ¹³C
558 and δ ¹⁸O values range between 2.27 and 3.76‰ and between 20.23 and 22.51‰, respectively. The δ ¹³C
559 and δ ¹⁸O values for the bedded travertine samples BV13 and BV11 differs from the others and show the
560 lowest δ ¹³C values and the highest δ ¹⁸O values. The δ ¹³C values of the banded travertines are high
561 (between 3.54 and 3.76‰), while their δ ¹⁸O values vary between 20.23 and 22.17 δ ¹⁸O‰.
562
563
564
565
566

567 The clumped isotope measurement was applied to a sample consisting of a banded calcite vein (BV
568 10), collected in the Quarry 2, (Figs 10 and 11), in order to reconstruct the palaeotemperature of the
569 hydrothermal fluids that were channeled through the faults. The same sample was also analysed through
570 U-Th radiometric dating (see the next paragraph). The powder sample (2 aliquots of BV 10, each 6-8 mg)
571 were analysed at the IsoLab, University of Washington, Seattle, WA, USA, using the procedures of
572 Burgener et al. (2016), Schauer et al. (2016) and Kelson et al. (2017). Powdered calcite was reacted in a
573 common acid bath at 90°C and purified using an automated system. Purified CO₂ was analysed using a
574 Thermo MAT253 isotope ratio mass spectrometer. Following Schauer et al. (2016), IUPAC parameters were
575 used to correct for ¹⁷O interference (Brand et al., 2010). Pressure baseline correction (He et al., 2012) was
576 made by measuring the reference gas signal 0.0084V down voltage of the mass 46 peak center. Clumped
577 isotope values (Δ47) are referenced to the carbon dioxide equilibrium scale, or absolute reference frame
578 Δ47 reference frame (Dennis et al., 2011) using CO₂ equilibrated at 4, 60 and 1000 °C. Temperatures were
579 calculated from measured Δ47 values using the calibration of Kelson et al. (2017), which was generated in
580 the same laboratory as our sample data.
581
582
583
584

585 Results of the clumped isotope measurements are summarized in Table 2. The determined average
586 Δ47 value is 0.588±0.021‰. The corresponding temperatures were calculated using of the equation of
587 Kelson et al. (2017) resulting 32° C. In course of the Δ47 measurement stable oxygen and carbon isotopic
588 values of the samples were also measured (Table 2).
589

590 δ¹⁸O of the precipitating water was calculated for the BV10 sample using the temperature
591 dependence of the calcite-water oxygen isotope fractionation (equations of Kim and O'Neil, 1997; Coplen,
592 2007 and Kele et al., 2015), the T_{Δ47} and the δ ¹⁸O_{carbonate} values.
593
594
595
596

597 4.2.4 U-Th dating

598
599
600

601
602
603
604
605
606
607
608
609
610
611
612
613
614
615
616
617
618
619
620
621
622
623
624
625
626
627
628
629
630
631
632
633
634
635
636
637
638
639
640
641
642
643
644
645
646
647
648
649
650
651
652
653
654
655
656
657
658
659
660

Key samples from the travertine deposit and from the calcite veins of the main faults zones have been collected in the different quarries and surroundings for datings (Fig. 10, Tab. 1). The age of the bedded travertine deposit has been defined collecting samples from the lower (S.U0) and upper (S.U10) units exposed in the quarries 1 and 3, respectively. The uppermost unit (S.U11) was not sampled as composed by not suitable travertine lithofacies, too altered for analysis. Samples of the banded calcite veins have been collected in order to reconstruct the age of the fluids circulation within the fault zones. We performed U-Th dating analyses using two different techniques: α spectrometry performed at the Laboratorio di Geochimica Ambientale e Isotopica of Roma Tre University (Italy), and Thermo Electron Neptune multi-collector inductively coupled mass spectrometer (MC-ICP-MS) (Shen et al., 2012) at the High-Precision Mass Spectrometry and Environment Change Laboratory (HISPEC) of the National Taiwan University, Taipei (Taiwan ROC).

For α spectrometry, we dissolved around 60 g of sample in 7 N HNO₃, filtering the solution to remove the insoluble residue. After adding hydrogen peroxide to destroy organic matter, the leachate was heated at 200 °C and then spiked with a ²²⁸Th–²³²U tracer. U and Th isotopic complexes were extracted following the procedure described in Edwards et al. (1988) and alpha-counted using high-resolution ion-implanted Ortec silicon-surface barrier detectors. Due to the presence of detrital non-radiogenic ²³⁰Th, ages obtained for samples with a ²³⁰Th/²³²Th activity ratio lower than or equal to 50 were corrected assuming an average ²³⁰Th/²³²Th activity ratio of 0.85 ± 0.36 (Wedepohl, 1995), which is the crustal thorium mean composition. We then calculated the ages using ISOPLOT, a plotting and regression program for radiogenic-isotope data (Ludwig, 2003).

For MC-ICP-MS dating, about 0.05 g of sample were covered with H₂O and gradually dissolved with double distilled 14 N HNO₃. After dissolution, we added a ²²⁹Th–²³³U–²³⁶U spike (Shen et al., 2003) to the sample, followed by 0.5 ml of HClO₄ to decompose the organic matter. We then followed the chemical procedure described in Shen et al. (2003) for the separation of uranium and thorium for instrumental analysis on MC-ICP-MS (Shen et al., 2012). We calculated the age correction using an estimated atomic ²³⁰Th/²³²Th ratio of 4±2 ppm. These latter value is typical for a material at secular equilibrium with the crustal ²³²Th/²³⁸U value of 3.8. We arbitrarily assumed a 50% error.

U-Th geochronology results are summarized in Table 3. The age of the travertine deposit ranges from 160.6 ± 6.6 ka to 22.1 ± 5.2 ka as deduced by the analyses of samples BV3 and BV13 (Fig. 10a; Tab. 3). Samples collected in the banded calcite vein network recognised in Quarry 2 (Figs 10 and 11) indicate that the S.U0 was affected by faulting ~ 23.3 ± 0.6 ka; faulting deformed the same rock volume and also the overlying S.U1 deposit until 9.5 ± 1.8 ka (Table 3 and Fig. 11), therefore suggesting fault activity during travertine deposition for at least 13 ka. This time span also includes the development of the palaeosoil and the angular unconformity separating S.U0 from the overlying S.U1 deposit (Fig. 11). Other banded calcite veins collected in Quarry 3 and surroundings (Fig. 10a) show ages that are in agreement with this time span, suggesting fault activity comprised between 14.3 ± 0.4 ka and 9.5 ± 1.3 ka (Table 3 and Fig. 10a).

5. Discussion

661
662 Our discussion is focused on: a) structural setting and tectonic control on fluid circulation; b) inferred
663 relationships between travertine deposition and faulting, and their age constraints; and c) consideration of
664 the regional tectonic and seismotectonic setting.
665
666
667

668 5.1 Tectonic control on fluids circulation and travertine deposition 669 670

671 The strict relation among thermal springs, travertine deposition and tectonic activity has been widely
672 documented by several authors in the last decades (Hancock et al., 1999; Altunel and Hancock, 1993a,
673 1993b; Çakır, 1999; Hancock et al., 1999; Brogi, 2004b; Altunel and Karabacak, 2005; Uysal et al., 2007, 2009;
674 Mesci et al., 2008; Brogi and Capezzuoli, 2009, 2014; Temiz et al., 2009, 2013; Brogi et al., 2010b, 2016; Temiz
675 and Eikenberg, 2011; Alçiçek et al., 2017; Claes et al., 2017; Henchiri et al., 2017; Berardi et al., 2016; Brogi
676 et al., 2017; 2018; Karabacak et al., 2019). These authors underline the role of travertine deposits in
677 recording tectonic activity through time in geothermal areas. Fluid circulation and upwelling overall in
678 geothermal systems (Barbier, 2002) depends on the permeability induced by bedrock fractures (Caine et
679 al., 1996; Cox et al., 2001): interconnection of micro- and macro-fractures control the pathways of
680 hydrothermal fluids (Zucchi et al., 2017), suggesting that faults related-damage in rock volumes plays a
681 major role in controlling hydrothermal fluids flow in upper crustal levels. Damage may be enhanced (and
682 therefore fluid flow channelled) where faults link, cross-cut each-other, and intersect (Kim et al., 2003),
683 thus influencing the location of thermal springs (Curewitz and Karson, 1997). As previously described, in
684 the study area travertine deposition was (and is) mainly controlled by the NE-trending faults, overall
685 where NE-trending faults intersect the NW-trending ones; in fact, fissure ridges-type travertine deposits
686 and mounds developed along both fault trends and nearby their intersection. Travertine deposition at the
687 intersection of NW(i.e. normal)- and NE(i.e. transfer)-trending faults is a common feature also for the
688 surroundings areas, as described for the Monte Amiata region (Brogi, 2008a; Brogi and Fabbrini, 2009;
689 Rimondi et al., 2015; Vignaroli et al., 2016), Rapolano Terme area (Brogi, 2004b) and Monte Cetona area
690 (Brogi et al., 2012), as well as worldwide (e.g. New Zeland, Rowland and Sibson, 2004; western Anatolia,
691 Alcicek et al., 2013).
692
693
694
695
696
697
698
699

700 5.2 Age of faulting, tectonic activity, palaeofluid temperatures and CO₂ origin 701 702

703 Fissure ridges and banded calcite veins occurrence across travertine deposits and substratum present
704 an excellent opportunity for reconstructing the age of faulting (Hancock et al., 1999; Altunel and
705 Karabacak, 2005; Uysal et al., 2007; Karabacak et al., 2019). Travertine deposition originates from fluids
706 with high sealing capacity that tends to decrease the fault permeability in absence of tectonic activity or
707 seismic events (Muir-Wood, 1993; Curewitz and Karson, 1997; Hancock et al. 1999; Micklethwaite and
708 Cox, 2004; Anderson and Fairley, 2008). As a result, travertine deposition occurs during tectonically active
709 periods (Brogi and Capezzuoli, 2014; Brogi et al., 2018; Karabacak et al., 2019; Williams et al., 2017), if
710 climate is favourable (Faccenna et al., 2008), and the age of travertine deposits can reveal much about the
711 age of faulting (Hancock et al., 1999; Uysal et al., 2007).
712
713

714 The analysis of the internal architecture of the travertine deposits, in terms of geometrical setting of
715 their different depositional units and facies, can provided information for the reconstruction of the
716 original morphology of the travertine body and feeder systems, represented by fissure ridges, mounds and
717
718
719
720

721
722 banded calcite veins. Our data indicate that the feeder systems were controlled by both NW- and NE-
723 trending faults delimiting the Poggione hill to the west and south, respectively (Fig, 6). The flowing
724 waters deposited the travertine beds on neighbouring slopes and morphological depressions (Fig. 9).

726 Banded calcite veins are consequence of crack-and-seal processes (Sibson, 1987), indicative of
727 repeated fracture opening pulses and contemporaneous fluids flow (Altunel and Karabakak, 2005; Uysal et
728 al. 2009; Brogi et al., 2016, 2017; Capezzuoli et al., 2018), accompanied by aragonitic-calcitic laminae
729 deposition. If this view, each lamina forming the banded veins recognised in the Quarries 2 and 3 should
730 be deposited in correspondence of a tectonic pulse, therefore revealing its age. Orientation of the banded
731 calcite veins (NW- and NE-trending) is parallel to the fissure ridges, matching the main faults trend as
732 recognised in the whole study area (Fig. 3 and 6a).

735 The radiometric ages obtained from the banded calcite veins developed along the NE-trending faults
736 system range from 23.3 ± 0.6 ka to 9.5 ± 1.8 ka, indicating fluids-assisted tectonic activity for at least 13 ka
737 (Fig. 10a and 11, Table 3). The banded calcite veins developed along the NW-trending fault indicate
738 activity between at least 14.3 ± 0.4 ka and 9.5 ± 1.3 (Figs 10a and 12, Table 3), suggesting that the two
739 fault systems were coeval, at least during the last period of their tectonic activity, with the NE-trending
740 faults documenting a longer history of crack and seal processes. Nevertheless, the age of the travertine
741 deposits suggests that the activity of both fault systems may have initiated earlier: the lower and older
742 depositional unit (S.U0), fed by the NE and NW-trending fissure ridges, have been dated at 160.6 ± 6.6 ka
743 (Table 3). This fact suggests that fault permeability and hydrological conditions favoured travertine
744 deposition since the latest middle Pleistocene. It is possible that faults activity started before the
745 travertine deposition giving the tendency of faults to become permeable during their mature stage (c.f.
746 Caine et al., 1996).

750 In contrast, deposition of the youngest age of travertine deposit (S.U10) was associated with fluids
751 flow from fissure ridge B that was active until at least 22.1 ± 5.2 ka. Ages of NW-trending banded
752 travertine veins suggest a younger age of fluid circulation, at least until 9.5 ± 1.3 ka.

754 Fluid flow and travertine deposition is still active in the eastern side of the study area, along the NE-
755 trending fault system (Figs 3 and 6). Travertine deposition implies that some faults segments are still
756 permeable; their permeability is possibly maintained by the widespread low-magnitude seismicity
757 recorded in the area (<http://cnt.rm.ingv.it/>).

759 Temperature of hydrothermal fluid that circulated within the fault zones, as determined through
760 clumped isotopes method (32°C) and the $\delta^{18}\text{O}$ using the temperature dependence of the calcite-water
761 oxygen isotope fractionation (equations of Kim and O'Neil, 1997; Coplen, 2007 and Kele et al., 2015), is in
762 the range of the Present fluids flowing from the active thermal springs in the Quarry 3. This result
763 suggests that the geothermal system did not change through time, at least considering water
764 temperature. The use of the equation of Kim and O'Neil (1997) resulted -5.63‰ , while the use of Coplen
765 (2007) and Kele et al. (2015) resulted lower $\delta^{18}\text{O}_{\text{water}}$ values (-7.41‰ and -8.49‰ , respectively). These
766 calculations demonstrate that the calculated $\delta^{18}\text{O}_{\text{water}}$ values depend strongly upon the equation used.
767 Kele et al. (2015) noted that in several travertine systems mineral-water oxygen isotope fractionation is
768 usually higher than that computed by the equation of Kim and O'Neil (1997). Thus, $\delta^{18}\text{O}_{\text{water}}$ it was most
769 probably lower than -5.63‰ . The $\delta^{18}\text{O}_{\text{water}}$ value of the Bagno Vignoni thermal spring is -7.9‰ (Fancelli
770 and Nuti, 1974) and present thermal springs in the area show similar values. Therefore, our isotopic data
771 suggest that the parent fluids of the travertine deposits and banded calcite veins show isotopic
772 composition similar to the present thermal springs. It must be further noted that the $\delta^{18}\text{O}_{\text{water}}$ values of
773
774
775
776
777

781
782 the present precipitation in the area is about -7‰ (Rimondi et al., 2015). Thus, travertines and banded
783 calcite veins at Bagno Vignoni could have been deposited from meteoric-derived fluids heated by the
784 regional geothermal anomaly. Their uprising, of course, is favoured by the faults-induced permeability.
785

786 Based on their positive $\delta^{13}\text{C}$ values (Table 2) the studied calcite vein and travertine samples are of
787 thermogene origin using the nomenclature of Pentecost (2005); their $\delta^{13}\text{C}$ values might be indicative of
788 the origin of CO_2 sources. The use of the empirical equation of Panichi and Tongiorgi (1976) resulted
789 $\delta^{13}\text{C}_{\text{CO}_2}$ values between -7.8 and -6 ‰ (V-PDB). The theoretical equation of Bottinga (1968) provided
790 similar $\delta^{13}\text{C}_{\text{CO}_2}$ values ranging between -7.1 and -5.7 ‰ (V-PDB) assuming equilibrium fractionation and
791 using the $\delta^{13}\text{C}$ values of travertines and the calculated $T_{\delta_{47}}$ (32 °C) of the BV 10 sample. The CO_2 coming
792 from magmatic sources has generally very low $\delta^{13}\text{C}$ values (from -7‰ to -5‰; Hoefs, 1997, Kele et al.,
793 2011), thus our calculations using both equations might indicate a deep, mantle origin for the CO_2 .
794
795
796
797
798
799

800 5.3 Regional and seismotectonic considerations 801

802
803 The NE-trending faults recognised in the study area define a wide shear zone, up to 3 km wide (Fig.
804 3) that is part of the transfer zone known as the Grosseto-Pienza tectonic lineament (Fig. 2). This is one
805 of the first order NE-trending (Fig.1) shear zone described for the inner zone of the Northern Apennines; it
806 crosses the inner zone of the belt (Boccaletti et al., 1977; Bemporad et al., 1986; Liotta, 1991) and played a
807 role in controlling the Neogene geological evolution of the southern Tuscany and the Northern Tyrrhenian
808 Sea (Ghelardoni, 1965; Bortolotti, 1966; Pascucci et al., 1999; 2007; Dini et al., 2008; Liotta et al., 2015;
809 Rosenbaum and Agostinetti, 2015). Inland, the Grosseto-Pienza tectonic lineament consists of a
810 continuous morpho-structural lineament (at least 100km long) delimiting, to the north, the Monte Amiata
811 Geothermal area, and crossing the Siena-Radicofani Basin (Fig. 2) giving rise to the “Pienza threshold”
812 that delimits the deeper (southern) basin, referred to as Radicofani Basin, with respect to the shallower
813 (northern) one, named as Siena Basin (Liotta and Salvatorini, 1994; Liotta, 1996; Pascucci et al., 2007).
814
815
816

817 Few data are available on the setting of structures that define such a transfer zone. Some minor
818 structures forming the Grosseto-Pienza tectonic lineament have been described in the Monte Leoni and
819 Paganico areas (Fig. 2), where NE-trending faults characterised by strike-slip to oblique-slip movements
820 have been documented (Aldinucci et al., 2008; Brogi and Fulignati, 2012). Additional data are from Pienza
821 area within the Radicofani Basin (Piccardi et al., 2017). The study area, located along the Grosseto-Pienza
822 tectonic lineament, intersects the western shoulder of the Pliocene Basin, where it divided in its northern
823 (Siena) and southern (Radicofani) part (Fig. 2).
824

825 Coexistence of NE-trending, left-lateral strike- to oblique-slip faults, and NW-trending normal faults
826 has been documented in the outcrops of the basin substratum (Fig. 3). Nevertheless, the Siena and
827 Radicofani basin ended its development during the middle Pliocene (Liotta, 1996; Pascucci et al., 2007;
828 Brogi, 2011), suggesting that the NW-trending faults bounding the basin were no-more active during
829 Quaternary. Conversely, we have documented the Pleistocene-Holocene age for the local NE-trending
830 faults, implying their later/younger activity. These structures have been active even after the development
831 of the Pliocene Basin. This can be once again explained considering the NE-trending structures as
832 belonging to the regional transfer zone, now accommodating extension in the easternmost sector of the
833 chain (Fig. 1). In this scenario, we do not exclude that some NW-trending fault segments, nearby or
834
835
836
837
838
839
840

841
842 within the NE-trending shear zone, were reactivated during Quaternary, as it was the case during the
843 travertine deposition and fissure ridges development (Fig. 3).
844

845 This tectonic scenario agrees to (i) the structural setting documented for the Monte Amiata area (Fig.
846 2), where Pleistocene-Holocene NE-trending faults influenced the volcanic centres localization and still
847 control the geothermal fluids circulation (Brogi and Fabbrini, 2009), and (ii) to the tectonic framework
848 defined for the Sarteano area (Fig. 2) where Quaternary NE-trending faults partially reactivated the
849 Pliocene faults (Brogi et al., 2012).
850

851 Concerning the seismotectonics, our observations allow to confirm that the Grosseto-Pienza tectonic
852 lineament is affected by recent-Present deformation, at least in the study sector. This is not in contrast
853 with the observation by Piccardi et al. (2017) who highlighted active/capable faults in the surroundings of
854 the study area. On the other hand, low-magnitude seismicity ($M < 4$) is recorded along the whole Grosseto-
855 Pienza tectonic lineament, (<http://cnt.rm.ingv.it>) and in particular in the study area, where seismic events
856 occurred in March 2018 nearby Bagno Vignoni (at least 22 events, $M < 3$). In this view, our data add useful
857 information to better constrain the palaeoseismicity and neotectonic activity, as well as the
858 seismotectonic context of this part of southern Tuscany.
859
860
861
862
863

864 6. Conclusions

865
866 Widespread long-lived (since 160 ka, at least) hydrothermal fluid circulation and travertine deposition
867 took place along the wide (at least 3 km) Grosseto-Pienza NE-trending tectonic lineament, active during
868 the development of the Neogene-Quaternary extension affecting the inner Northern Apennines. The
869 palaeo-temperature and the isotopic composition of the hydrothermal fluids are similar to those of
870 present-day thermal springs, accounting for a common tectonic scenario through time. This transfer zone
871 is still active and able to produce low-magnitude ($M < 4$) seismicity; such a setting has an important fallout
872 for the seismic hazard assessment of southern Tuscany.
873
874

875 Travertine deposits formed from thermal springs aligned along transfer zone-fault segments and at
876 their intersections with NW-trending faults. Faults permeability was guaranteed by the enhanced
877 damaging at the intersection with the still active NE-trending faults that reopened the sealed fractures
878 gaining a renewed permeability. The study of the travertine deposits, in terms of their architectural
879 setting, facies distribution, ages and isotopic composition was essential for reconstructing the activity of
880 faults, their permeability evolution and palaeo-fluids features. In this view, banded calcite veins offered
881 the best opportunity to reconstruct the interplay between faulting, permeability evolution and fluids-flow
882 in all geothermal areas characterised by bicarbonate-rich geothermal fluids. This picture underlines the
883 role of the travertine deposits in reconstructing the neotectonic settings in geothermal areas.
884
885
886
887
888

889 Acknowledgments

890
891 Support of the KH 125584 project (NKFIH, National Research, Development and Innovation Office,
892 Hungary), the TraRAS (Travertine Reservoir Analogue Studies) project, as well as the support of the
893 European Union and the State of Hungary, co-financed by the European Regional Development Fund in
894 the project of GINOP-2.3.2-15-2016-00009 'ICER' are gratefully acknowledged by S.K. E.C. is pleased to
895 acknowledge a P.O.R.-F.S.E. 2007-2013 (Regional Competitiveness and Employment) grant from the
896
897
898
899
900

901
902 Tuscan Regional Administration. U-Th dating was supported by the Ministry of Science and
903 Technology (MOST) (107-2119-M-002-051 to C.-C.S.), the National Taiwan University (105R7625
904 to C.-C.S.), the Higher Education Sprout Project of the Ministry of Education, Taiwan ROC
905 (107L901001 to C.-C.S.). We also acknowledge U.S. National Science Foundation grant EAR-
906 1156134 to K.W.H.
907
908
909
910
911

912 913 References

- 914
915 Acocella, V., Funiciello, R., 1999. The interaction between regional and local tectonics during resurgent
916 doming: the case of the island of Ischia, Italy. *Journal of Volcanology and Geothermal Research* 88,
917 109-123.
918
- 919 Acocella, V., Funiciello, R., 2002. Transverse structures and volcanic activity along the Tyrrhenian margin
920 of central Italy. *Boll.Soc.Geol.Ital.* 1, 739-747.
921
- 922 Acocella, V., Funiciello, R., 2006. Transverse systems along the extensional Tyrrhenian margin of central
923 Italy and their influence on volcanism. *Tectonics*, 25. <http://dx.doi.org/10.1029/2005TC001845>.
924
- 925 Albarello, D., Batini, F., Bianciardi, P., Ciulli, B., Spinelli, E., Viti, M., 2005. Stress field assessment from ill-
926 defined fault plane solutions: an example from the Larderello Geothermal Field (western Tuscany,
927 Italy). *Boll. Soc. Geol. It* 3, 187-193.
928
- 929 Alçiçek, M.C., Brogi, A., Capezzuoli, E., Liotta, D., Meccheri, M., 2013. Superimposed basins formation
930 during the Neogene-Quaternary extensional tectonics in SW-Anatolia (Turkey): insights from the
931 kinematics of the Dinar Fault Zone. *Tectonophysics* 608, 713-727.
932
- 933 Alçiçek, M.C., Alçiçek, H., Altunel, E., Arenas, C., Bons, P., Brogi, A., Capezzuoli, E., de Riese, T., Della
934 Porta, G., Gandin, A., Guo, Li, Jones, B., Karabacak, V., Kershaw, S., Liotta, D., Mindszenty, A., Pedley,
935 M., Ronchi, P., Swennen, R., Temiz, U., 2017. Comment on “First records of syn-diagenetic non-tectonic
936 folding in Quaternary thermogene travertines caused by hydrothermal incremental veining” by Billi et
937 al. *Tectonophysics* 721, 491-500.
938
- 939 Aldinucci, M., Pandeli, E., Sandrelli, F., 2008. Tectono-sedimentary evolution of the Late Palaeozoic-Early
940 Mesozoic metasediments of the Monticiano-Roccastrada Ridge (southern Tuscany, Northern
941 Apennines, Italy). *Boll. Soc. Geol. It* 127, 567-579.
942
- 943 Altunel, E., Hancock, P.L., 1993a. Active Fissuring and Faulting in Quaternary Travertines at Pamukkale,
944 Western Turkey. In: Stewart, I.S., Vita-Finzi, C., Owen, L.A. (Eds.), *Neotectonics and Active Faulting:*
945 *Zeitschrift Fuer Geomorphologie Supplement Vol. 94*, pp. 285-302.
946
- 947 Altunel, E., Hancock, P.L., 1993b. Morphology and structural setting of Quaternary travertines at
948 Pamukkale, Turkey. *Geol. J.* 28, 335-346.
949
- 950 Altunel, E., Hancock, P.L., 1996. Structural attributes of travertine-filled extensional fissures in the
951 Pamukkale Plateau, Western Turkey. *Int. Geol. Rev.* 38, 768-777.
952
- 953 Altunel, E., Karabacak, V., 2005. Determination of horizontal extension from fissure-ridge travertines: a
954 case study from the Denizli Basin, southwestern Turkey. *Geodin. Acta* 18, 333-342.
955
- 956 Anderson, T., R., Fairley, J., P., 2008. Relating permeability to the structural setting of a fault-controlled
957 hydrothermal system in southeast Oregon, USA. *Journal of Geophysical Research* 113,
958 doi:10.1029/2007JB004962.
959
960

- 961
962
963 Bally, A., W., 1981. Atlantic type margins, in *Geology of passive continental margins: history, structure*
964 *and sedimentologic record: AAPG. Education Course Notes Series 19*, p. 1–48.
- 965 Barbier, E., 2002. Geothermal energy and current status: An overview. *Renew Sus Energy Rev* 6, 3–65.
- 966
967 Barchi, M.,R., De Feyter, A.,J., Magnani, M.,B., Minelli, G., Piali, G., Sotera, B.,M., 1998. Extensional
968 tectonics in the Northern Apennines (Italy): evidence from the Crop03 deep seismic reflection line.
969 *Mem. Soc. Geol. It.* 52, 527–538.
- 970
971 Barchi, M., R., 2010. The Neogene–Quaternary evolution of the Northern Apennines: crustal structure,
972 style of deformation and seismicity. *Journal of the Virtual Explorer*, 36,
973 <https://doi.org/10.3809/jvirtex.2009.00220>
- 974
975 Bartole, R., 1995. The North-Tyrrhenian–Northern Apennines post-collisional system: constraints for a
976 geodynamic model. *Terranova* 1, 7–30.
- 977
978 Batini, F., Brogi, A., Lazzarotto, A., Liotta, D., Pandeli, E., 2003. Geological features of Larderello–Travale
979 and Mt Amiata geothermal areas (southern Tuscany Italy). *Episodes* 26, 239–244.
- 980
981 Bemporad, S., Conedera, C., Dainelli, P., Ercoli, A. and Facibeni, P., 1986. Landsat imagery: a valuable
982 tool for regional and structural geology. *Mem. Soc. Geol. Ital.* 31 , 287–298.
- 983
984 Berardi, G., Vignaroli, G., Billi, A., Rossetti, F., Soligo, M., Kele, S., Baykara, M., O., Bernasconi, S., M.,
985 Castorina, F., Tecce, F., Shen, C., 2016. Growth of a Pleistocene giant carbonate vein and nearby
986 thermogene travertine deposits at Semproniano, southern Tuscany, Italy: Estimate of CO₂ leakage.
987 *Tectonophysics* 690, 219-239.
- 988
989 Bianchi, V., Ghinassi, M., Aldinucci, M., Boaga, J., Brogi, A., Deiana, R., 2015. Tectonically driven
990 deposition and landscape evolution within upland incised valleys: Ambra Valley fill, Pliocene–
991 Pleistocene, Tuscany, Italy. *Sedimentology* 62, 897–927.
- 992
993 Bianco, C., Brogi, A., Caggianelli, A., Giorgetti, G., Liotta, D., Meccheri, M., 2015. HP-LT metamorphism in
994 Elba Island: Implications for the geodynamic evolution of the inner Northern Apennines (Italy). *Journal*
995 *of Geodynamics* 91, 13-25.
- 996
997 Boccaletti, M., Elter, P., Guazzone, G.J.P., 1971. Plate tectonic models for the development of the western
998 Alps and Northern Apennines. *Nature* 234, 108–111.
- 999
1000 Boccaletti, M., Fazzuoli, M., Loddo, M., Mongelli, F., 1977. Heat flow measurements on the Northern
1001 Apennines Arc. *Tectonophysics*, 41 101-112.
- 1002
1003 Bonini, M., Moratti, G., 1995. Evoluzione tettonica del bacino neogenico di Radicondoli-Volterra (Toscana
1004 meridionale). *Boll. Soc. Geol. It.* 114, 549–573.
- 1005
1006 Bonini, M., Sani, F., 2002. Extension and compression in the northern Apennines (Italy) hinterland:
1007 evidence from the late Miocene-Pliocene Siena-Radicofani Basin and relations with basement
1008 structures. *Tectonics* 22, 1–35.
- 1009
1010 Bonini, L., Di Bucci, D., Toscani, G., Seno, S., Valensise, G., 2014. On the complexity of surface ruptures
1011 during normal faulting earthquakes: excerpts from the 6 April 2009 L'Aquila (central Italy) earthquake
(Mw 6.3). *Solid Earth* 5, 389-408.
- 1012
1013 Bortolotti, V., 1966. La tettonica trasversale dell'Appennino. I-La linea Livorno-Sillaro, *Boll. Soc. Geol. It.*,
1014 85, 529-540.
- 1015
1016 Bossio, A., Costantini, A., Lazzarotto, A., Liotta, D., Mazzanti, R., Mazzei, R., Salvatorini, G., Sandrelli, F.,
1017 1993. Rassegna delle conoscenze sulla stratigrafia del Neoauctono Toscano. *Mem. Soc. Geol. Ital.* 49,
1018 17–98.

- 1021
1022
1023 Bottinga, Y. 1968. Calculation of fractionation factors for carbon and oxygen isotopic exchange in the
1024 system calcite–carbon dioxide–water. *Journal of Physical Chemistry*, 72, 800–808.
1025
- 1026 Brand, W., A., Assonov, S., S., Coplen, T., B., 2010. Correction for the ^{17}O interference in $\delta^{13}\text{C}$
1027 measurements when analyzing CO_2 with stable isotope mass spectrometry (IUPAC Technical Report).
1028 *Pure Appl. Chem.* 82, 1719–1733.
1029
- 1030 Brogi, A., 2004a. Miocene low-angle detachments and upper crust megaboudinage in the Monte Amiata
1031 geothermal area (Northern Apennines, Italy). *Geodinamica Acta* 17/6, 375–387.
1032
- 1033 Brogi, A., 2004b. Faults linkage, damage rocks and hydrothermal fluid circulation: tectonic interpretation
1034 of the Rapolano Terme travertines (southern Tuscany, Italy) in the context of the Northern Apennines
1035 Neogene–Quaternary extension. *Eclogae Geol. Helv.* 97, 307–320.
1036
- 1037 Brogi, A., 2006. Neogene extension in the Northern Apennines (Italy): insights from the southern part of
1038 the Mt Amiata geothermal area. *Geodinamica Acta* 19, 33–50.
1039
- 1040 Brogi, A., 2008a. The structure of the Monte Amiata volcano-geothermal area (Northern Apennines, Italy):
1041 Neogene–Quaternary compression versus extension. *International Journal of Earth Sciences* 97, 677–
1042 703.
1043
- 1044 Brogi, A., 2008b. Kinematics and geometry of Miocene low-angle detachments and exhumation of the
1045 metamorphic units in the hinterland of the Northern Apennines (Italy). *J. Struct. Geol.* 30, 2–20.
1046
- 1047 Brogi, A., 2011. Bowl-shaped basin related to low-angle detachment during continental extension: the case
1048 of the controversial Neogene Siena Basin (central Italy, Northern Apennines). *Tectonophysics* 499, 54–
1049 76.
- 1050 Brogi, A., Lazzarotto, A., Liotta, D., Ranalli, G., 2005a. Crustal structures in the geothermal areas of
1051 southern Tuscany (Italy): insights from the CROP18 deep seismic reflection lines. *J. Vol. Geoth. Res.*
1052 148, 60–80.
1053
- 1054 Brogi, A., Lazzarotto, A., Liotta, D., CROP 18 Working Group, 2005b. Structural features of southern
1055 Tuscany and geological interpretation of the CROP 18 seismic reflection survey, Italy. *Boll. Soc. Geol. It*
1056 3, 213–236.
1057
- 1058 Brogi, A., Cornamusini, G., Sandrelli, F., 2005c. Geological setting of the Bagno Vignoni area (Northern side
1059 of the Mt. Amiata geothermal area, Italy): collisional structures recorded in Tuscan Nappe. *Boll. Soc.*
1060 *Geol. It., Vol. Spec.* 3, 89–101.
1061
- 1062 Brogi, A., Lazzarotto, A., Grassi, S., 2007. The Bagno Vignoni 1 borehole log (Northern Mt. Amiata
1063 geothermal area, Southern Tuscany). *Rend. Soc. Geol. It.* 5, 84–87.
1064
- 1065 Brogi, A., Liotta, D., 2008. Highly extended terrains, lateral segmentation of the substratum, and basin
1066 development: the Middle–Late Miocene Radicondoli Basin (inner northern Apennines, Italy). *Tectonics*,
1067 27, TC5002.
1068
- 1069 Brogi, A., Capezzuoli, E., 2009. Travertine deposition and faulting: the fault-related travertine fissure-ridge
1070 at Terme di S.Giovanni, Rapolano Terme (Italy). *Int. J. Earth Sci.* 98, 931–948.
1071
- 1072 Brogi, A., Fabbrini, L., 2009. Extensional and strike-slip tectonics across the Monte Amiata–Monte Cetona
1073 transect (Northern Apennines, Italy) and seismotectonic implications. *Tectonophysics* 476, 195–209.
1074
- 1075 Brogi, A., Liotta, D., Meccheri, M., Fabbrini, L., 2010a. Transtensional shear zones controlling volcanic
1076 eruptions: the Middle Pleistocene Monte Amiata volcano (inner Northern Apennines, Italy). *Terra Nova*
1077 22, 137–146.
1078
1079
1080

- 1081
1082
1083 Brogi, A., Capezzuoli, E., Aqué, R., Branca, M., Voltaggio, M., 2010b. Studying travertine for neotectonics
1084 investigations: Middle–Late Pleistocene syntectonic travertine deposition at Serre di Rapolano
1085 (Northern Apennines, Italy). *Geologische Rundschau* 99, 1383–1398.
1086
1087 Brogi, A., Giorgetti, G., 2010. The tectono-metamorphic record of the Tuscan Nappe from the Colline
1088 Metallifere region (Northern Apennines, Italy). *Ital. J. Geosci.* 129, 177–187.
1089
1090 Brogi, A., Fabbrini, L., Liotta, D., 2011. Sb–Hg ore deposit distribution controlled by brittle structures: The
1091 case of the Selvena mining district (Monte Amiata, Tuscany, Italy). *Ore Geology Reviews* 41, 35–48.
1092
1093 Brogi, A., Fulignati, P., 2012. Tectonic control on hydrothermal circulation and fluid evolution in the
1094 Pietratonda–Poggio Peloso (southern Tuscany, Italy) carbonate-hosted Sb-mineralization. *Ore Geology*
1095 *Reviews* 44, 158–171.
1096
1097 Brogi, A., Capezzuoli, E., Buracchi, E., Branca, M., 2012. Tectonic control on travertine and calcareous tufa
1098 deposition in a low-temperature geothermal system (Sarteano, Central Italy). *Journal of the Geological*
1099 *Society, London*, 169, 461–476.
1100
1101 Brogi, A., Giorgetti, G., 2012. Tectono-metamorphic evolution of the siliciclastic units in the Middle Tuscan
1102 Range (inner Northern Apennines): Mg-carpholite bearing quartz veins related to syn-metamorphic
1103 syn-orogenic foliation. *Tectonophysics* 526–529, 167–184.
1104
1105 Brogi, A., Fidolini, F., Liotta, D., 2013. Tectonic and sedimentary evolution of the Upper Valdarno Basin:
1106 new insights from the lacustrine S. Barbara Basin. *Italian Journal of Geoscience* 132, 81–97.
1107
1108 Brogi, A., Capezzuoli, E., 2014. Earthquake impact on fissure-ridge type travertine deposition. *Geological*
1109 *Magazine* 151, 1135–1143.
1110
1111 Brogi, A., Capezzuoli, E., Martini, I., Picozzi, M., Sandrelli, F., 2014. Late Quaternary tectonics in the inner
1112 Northern Apennines (Siena Basin, southern Tuscany, Italy) and their seismotectonic implication.
1113 *Journal of Geodynamics* 76, 25–45.
1114
1115 Brogi, A., Alçiçek, M., C., Yalçiner, C.C., Capezzuoli, E., Liotta, D., Meccheri, M., Rimondi, V., Ruggieri, G.,
1116 Gandin, A., Boschi, C., Büyüksaraç, A., Alçiçek, H., Bülbül, A., Baykara, M.O., Shen, C.-C., 2016.
1117 Hydrothermal fluids circulation and travertine deposition in an active tectonic setting: Insights from
1118 the Kamara geothermal area (western Anatolia, Turkey). *Tectonophysics* 680, 211–232.
1119
1120 Brogi, A., Capezzuoli, E., Kele, K., Baykara, M., O., Shen, C., 2017. Key travertine tectofacies for
1121 neotectonics and palaeoseismicity reconstruction: effects of hydrothermal overpressured fluid
1122 injection. *Journal of Geological Society* 174(4), 679.
1123
1124 Brogi, A., Capezzuoli, E., Moretti, M., Olvera-García, E., Matera, P., F., Garduno-Monroy, V., Mancini, A.,
1125 2018. Earthquake-triggered soft-sediment deformation structures (seismites) in travertine deposits.
1126 *Tectonophysics* 745, 349–365.
1127
1128 Brunet, C., Monié, P., Jolivet, L., Cadet, J.P., 2000. Migration of compression and extension in the
1129 Tyrrhenian Sea, insights from ⁴⁰Ar/³⁹Ar ages on micas along a transect from Corsica to Tuscany.
1130 *Tectonophysics* 321, 127–155.
1131
1132 Buonasorte, G., Fiordelisi, A., Rossi, U., 1987. Tectonic structures and geometric setting of the Vulsini
1133 Volcanic Complex. *Periodico di Mineralogia* 56, 123–136. Burgener, L., Huntington, K., W., Hoke, G., D.,
1134 Schauer, A., Ringham, M., C., Latorre, C., Díaz, F., P., 2016. Variations in soil carbonate formation and
1135 seasonal bias over >4 km of relief in the western Andes (30°S) revealed by clumped isotope
1136 thermometry. *Earth Planet. Sci. Lett.* 441, 188–199.
1137
1138 Çakır, Z., 1999. Along-strike discontinuity of active normal faults and its influence on quaternary
1139 travertine deposition: examples from western Turkey. *Turkish Journal of Earth Sciences* 8, 67–80.
1140

- 1141
1142
1143 Caine S., J., Evans J., P., Forster C., B., 1996. Fault zone architecture and permeability structure. *Geology*
1144 24, 1025–1028.
1145
1146 Calamai, A., Cataldi, R., Squarci, P., Taffi, L., 1970. Geology geophysics and hydrogeology of the Monte
1147 Amiata geothermal field. *Geothermics* 1, 1–9.
1148
1149 Calcagnile, G., Panza, G., 1981. The main characteristics of the lithosphere asthenosphere system in Italy
1150 and surrounding regions, *Pure Appl. Geophys.* 119, 865-879.
1151
1152 Capezzuoli E., Gandin A., Pedley H.M., 2014. Decoding tufa and travertine (freshwater carbonates) in the
1153 sedimentary record: the state of the art. *Sedimentology*, 61, 1–21
1154
1155 Capezzuoli, E., Ruggieri, G., Rimondi, V., Brogi, A., Liotta, D., Alçiçek, M. C., Alçiçek, H., Bülbül, A.,
1156 Gandin, A., Meccheri, M., Shen, C-C., Baykara, M.O., 2018. Calcite veining and feeding conduits in a
1157 hydrothermal system: Insights from a natural section across the Pleistocene Gölemezli travertine
1158 depositional system (western Anatolia, Turkey). *Sedimentary Geology*, 364, 180–203.
1159
1160 Carmignani, L., Kligfield, R., 1990. Crustal extension in the Northern Apennines: transition from
1161 compression to extension in the Alpi Apuane core complex. *Tectonics* 9, 1275–1303.
1162
1163 Carmignani, L., Decandia, F., A., Disperati, L., Fantozzi, P., L., Lazzarotto, A., Liotta, D., Meccheri, M., 1994.
1164 Tertiary extensional tectonics in Tuscany (Northern Apennines Italy). *Tectonophysics* 238, 295– 315.
1165
1166 Carmignani, L., Decandia, F.A., Disperati, L., Fantozzi, P.L., Lazzarotto, A., Liotta, D., Oggiano, G., 1995.
1167 Relationships between the Sardinia–Corsica–Provencal Domain and the Northern Apennines. *Terra*
1168 *Nova* 7, 128–137.
1169
1170 Carmignani, L., Decandia, F.A., Disperati, L., Fantozzi P.L., Kligfield, R., Lazzarotto, A., Liotta, D., Meccheri,
1171 M., 2001. Inner Northern Apennines In: Vai GB, Martini IP (eds) *Anatomy of an orogen: the Apennines*
1172 *and adjacent Mediterranean basins*, Kluwer, Dordrecht.
1173
1174 Cadoux, A., Pinti, D.L., 2009. Hybrid character and pre-eruptive events of Mt Amiata volcano (Italy)
1175 inferred from geochronological, petro-geochemical and isotopic data. *Journal of Volcanology and*
1176 *Geothermal Research* 179, 169-190.
1177
1178 Cheng, H., Edwards. L.R., Shen, C.C., Polyak, V.J., Asmerom, Y., Woodhead, J., Hellstrom, J., Wang, Y.,
1179 Kong, X., Spötl, C., Wang, X., Calvin, A.E., 2013. Improvements in ²³⁰Th dating, ²³⁰Th and ²³⁴U half-
1180 life values, and U–Th isotopic measurements by multi-collector inductively coupled plasma mass
1181 spectrometry. *Earth and Planetary Science Letters* 371, 82–91.
1182
1183 Claes, H., Erthal, M.M., Soete, J., Özkul, M., Swennen, R., 2017. Shrub and pore type classification:
1184 Petrography of travertine shrubs from the Ballık-Belevi area (Denizli, SW Turkey). *Quaternary*
1185 *International* 437, 147-163.
1186
1187 Collettini, C., De Paola, N., Holdsworth, R.E., Barchi, M.R., 2006. The development and behaviour of low-
1188 angle normal faults during Cenozoic asymmetric extension in the Northern Apennines, Italy. *J. Struct.*
1189 *Geol.* 28, 333–352.
1190
1191 Coplen, T.B., 2007. Calibration of the calcite–water oxygenisotope geothermometer at Devils Hole,
1192 Nevada, a natural laboratory. *Geochim. Cosmochim. Acta* 71, 3948–3957.
1193
1194 Cox, S.F., Knackstedt, M.A., Braun, J., 2001. Principles of Structural Control on Permeability and Fluid
1195 Flow in Hydrothermal Systems (*Structural Controls on Ore Genesis*). Society of Economic Geologists
1196 24. pp. 1–24 Chapter 1.
1197
1198
1199
1200

- 1201
1202 Curewitz, D., Karson, J., A., 1997. Structural settings of hydrothermal outflow: fracture permeability
1203 maintained by fault propagation and interaction. *J. Volcanol. Geotherm. Res.* 79, 149–168.
1204
- 1205 Dallmeyer, R., D., Liotta, D., 1998. Extension, uplift of rocks and cooling ages in thinned crustal provinces:
1206 the Larderello geothermal area (inner northern Apennines, Italy). *Geol. Mag.* 135, 193–202.
1207
- 1208 Decandia, F., A., Lazzarotto, A., Liotta, D., (1993). La “Serie ridotta” nel quadro dell’evoluzione geologica
1209 della Toscana meridionale. *Mem. Soc. Geol. It.* 49, 181–190.
1210
- 1211 Dennis, K.J., Affek, H.P., Passey, B.H., Schrag, D.P., Eiler, J.M., 2011. Defining an absolute reference frame
1212 for ‘clumped’ isotope studies of CO₂. *Geochim. Cosmochim. Acta* 75 (22), 7117–7131.
1213
- 1214 Di Bucci, D., Mazzoli, S., 2002. Active tectonics of the Northern Apennines and Adria geodynamics: new
1215 data and a discussion. *Journal of Geodynamics* 34, 687–707.
1216
- 1217 Di Stefano, R., Chiarabba, C., Chiaraluce, L., Cocco, M., De Gori, P., Piccinini, D., Valoroso, L., 2011. Fault
1218 zone properties affecting the rupture evolution of the 2009 (Mw6.1) L’Aquila earthquake (central
1219 Italy): Insights from seismic tomography. *Geophysical Research Letters* 38, 110310,
1220 Doi:10.1029/2011gl047365
- 1221 Dini, A., Mazzarini, F., Musumeci, G., Rocchi, S., 2008. Multiple hydro-fracturing by boron-rich fluids in
1222 the Late Miocene contact aureole of eastern Elba Island (Tuscany, Italy). *Terra Nova*, 20, 318–326.
1223
- 1224 Doglioni, C., 1991. A proposal of kinematic modeling for W-dipping subductions. Possible applications to
1225 the Tyrrhenian-Apennines system. *Terra Nova* 3 (423), 434.
1226
- 1227 Ebinger, C.J., 1989. Geometric and kinematic development of border faults and accommodation zones,
1228 Kivu-Rusizi rift, Africa. *Tectonics*, 8, 117–137
1229
- 1230 Edwards, R.L., Chen, J.H., Wasserburg, G.J., 1988. ²³⁸U–²³⁴U–²³⁰Th systematics and the precise
1231 measurement of time over the last 500,000 years. *Earth Planet. Sci. Lett.* 81, 175–192.
1232
- 1233 Erthal, M. M., Capezzuoli, E., Mancini, A., Claes, H., Soete, J., Swennen, R. 2017. Shrub morpho-types as
1234 indicator for the water flow energy - Tivoli travertine case (Central Italy). *Sedimentary Geology*, 347,
1235 79–99.
1236
- 1237 Faccenna, C., Soligo, M., Billi, A., De Filippis, L., Funiciello, R., Rossetti, C., Tuccimei, P., 2008. Late
1238 Pleistocene depositional cycles of the Lapis Tiburtinus travertine (Tivoli, Central Italy): possible
1239 influence of climate and fault activity. *Glob. Planet. Chang.* 63, 299–308.
1240
- 1241 Ferrari, L., Conticelli, S., Burlamacchi, L., Manetti, P., 1996. Volcanological evolution of the Monte Amiata,
1242 Southern Tuscany: new geological and petrochemical data. *Acta Vulcanologica* 8, 41–56.
1243
- 1244 Finetti, I.R., Boccaletti, M., Bonini, M., Del Ben, A., Geletti, R., Pipan, M., Sani, F., 2001. Crustal section
1245 based on CROP seismic data across the North Tyrrhenian-Northern Apennines-Adriatic Sea.
1246 *Tectonophysics* 343, 135–163.
1247
- 1248 Finetti, I.R., 2006. Basic regional crustal setting and superimposed local pluton intrusion related tectonics
1249 in the Larderello-Monte Amiata geothermal province, from integrated CROP seismic data. *Boll. Soc.
1250 Geol. It.* 125, 117–146.
- 1251 Gandin, A., Capezzuoli, E., 2014. Travertine: distinctive depositional fabrics of carbonates from thermal
1252 spring systems. *Sedimentology* 61, 264–290.
1253
- 1254 Ghelardoni, G., 1965. Osservazioni sulla tettonica trasversale dell’Appennino settentrionale, *Boll. Soc.
1255 Geol. It.*, 93, 837–860.
1256
- 1257 Gibbs, A. D., 1990. Linked fault families in basin formation. *J. Struct. Geol.* 12, 795–803.
1258
1259
1260

- 1261
1262
1263 Gualtieri, L., Bertotti, G., Cloetingh, S., 1998. Lateral variation of thermo-mechanical properties in the
1264 Tyrrhenian Northern Apennine region. *Tectonophysics* 300, 143-158.
1265
1266 Guo, L., Riding, R., 1999. Rapid facies changes in Holocene fissure ridge hot spring travertines, Rapolano
1267 Terme, Italy. *Sedimentology*, 46, 1145–1158.
1268
1269 Hancock, P.L., Chalmers, R.M.L., Altunel, E., Çakır, Z., 1999. Travertines: using travertines in active fault
1270 studies. *J. Struct. Geol.* 21, 903–916.
1271
1272 He, B., Olack, G.A., Colman A.S., 2012. Pressure baseline correction and high-precision CO₂ clumped
1273 isotope ($\Delta 47$) measurements in bellows and micro-volume modes. *Rapid Commun. Mass Spectrom.* 26,
1274 2837–2853.
1275
1276 Henchiri, M., Ahmed, W.B., Brogi, A., Alçiçek, M.C., Benassi, R., 2017. Evolution of Pleistocene travertine
1277 depositional system from terraced slope to fissure-ridge in a mixed travertine-alluvial succession (Jebel
1278 El Mida, Gafsa, southern Tunisia). *Geodinamica Acta* 29, 20-41.
1279
1280 Hiess, J., Condon, D.J., McLean, N., Noble, S.R., 2012. U-238/U-235 Systematics in Terrestrial Uranium-
1281 Bearing Minerals. *Science* 335, 1610-1618.
1282
1283 Hoefs, J., 1997. *Stable Isotope Geochemistry*. Springer-Verlag, Berlin. 201 p.
1284
1285 Jolivet, L., Dubois, R., Fournier, R., Goffe', B., Michard, A., Jourdan, C., 1990. Ductile extension in alpine
1286 Corsica. *Geology* 18, 1007–1010.
1287
1288 Karabacak, V., Uysal, I.T., Mutlu, H., Ünal-İmer, E., Dirik, R.K., Feng, Y., Akiska, S., Aydoğdu, İ., Zhao, J.,
1289 2019. Are U-Th dates correlated with historical records of earthquakes? Constraints from co-seismic
1290 carbonate veins within the North Anatolian Fault Zone. *Tectonics* DOI:10.31223/osf.io/kbt6p.
1291
1292 Kele, S., Breitenbach, S.F.M., Capezzuoli, E., Meckler, A.N., Ziegler, M., Millan, I.M., Kluge, T., Deák, J.,
1293 Hanselmann, K., John, C.M., Yan, H., Liu, Z., Bernasconi, S.M., 2015. Temperature dependence of
1294 oxygen- and clumped isotope fractionation in carbonates: A study of travertines and tufas in the 6–95
1295 °C temperature range. *Geochimica et Cosmochimica Acta* 168, 172-192.
1296
1297 Kele, S., Özkul, M., Fózizs, I., Gökgöz, A., Baykara, M.O., Alçiçek, M.C., Németh, T., 2011. Stable isotope
1298 geochemical study of Pamukkale travertines: new evidences of lowtemperature non-equilibrium
1299 calcite-water fractionation. *Sediment. Geol.* 238, 191–212.
1300
1301 Kelson, J.R., Huntington, K.W., Schauer, A.J., Saenger, C., Lechler, A.R., 2017. Toward a universal carbonate
1302 clumped isotope calibration: Diverse synthesis and preparatory methods suggest a single temperature
1303 relationship. *Geochim. Cosmochim. Acta* 197, 104–131.
1304
1305 Kim, S.-T., O'Neil, J.R., 1997. Equilibrium and nonequilibrium oxygen isotope effects in synthetic
1306 carbonates. *Geochim. Cosmochim. Acta* 61, 3461–3475.
1307
1308 Kim, Y.-S., Peacock, D.C.P., Sanderson, D.J., 2003. Strike-slip faults and damage zones at Marsalforn, Gozo
1309 Island, Malta. *J. Struct. Geol.* 25, 793-812.
1310
1311 Kluge, T., John, C.M., Boch, R., Kele, S., 2018. Assessment of factors controlling clumped isotopes and
1312 $\delta 18\text{O}$ values of hydrothermal vent calcites. *Geochemistry, Geophysics, Geosystems* 19, 1844-1858.
1313
1314 Lavecchia, G., 1988. The Tyrrhenian-Apennines system: structural setting and seismotectogenesis.
1315 *Tectonophysics* 147, 263–296.
1316
1317
1318
1319
1320

- 1321
1322 Lavecchia, G., Boncio, P., Creati, N., Brozzetti, F., 2004. Stile strutturale stato termo-meccanico e
1323 significato sismogenetico del thrust adriatico: dati e spunti da una revisione del profilo CROP 03
1324 integrata con l'analisi di dati sismologici. *Boll. Soc. Geol. It.* 123, 111–126.
1325
1326 Lazzarotto, A., Mazzanti, R., 1978. Geologia dell'alta Val di Cecina. *Boll. Soc. Geol. It.* 95, 1365–1487.
1327
1328 Liotta, D., 1991. The Arbia-Val Marecchia Line, Northern Apennines. *Eclogae Geologicae Helvetiae* 84(2), 413-
1329 430.
1330
1331 Liotta, D., 1994. Structural features of the Radicofani basin along the Piancastagnaio (Monte Amiata)–
1332 S.Casciano dei Bagni (Monte Cetona) cross section. *Mem. Soc. Geol. It.* 48, 401–408.
1333
1334 Liotta, D., 1996. Analisi del settore centro-meridionale del Bacino pliocenico di Radicofani, Toscana
1335 meridionale. *Boll. Soc. Geol. Ital.* 115, 115–143.
1336
1337 Liotta, D., Salvatorini, G., 1994. Evoluzione sedimentaria e tettonica della parte centromeridionale del
1338 bacino pliocenico di Radicofani. *Studi Geol. Camerti Spec.* 1, 65–77.
1339
1340 Liotta, D., Ranalli, G., 1999. Correlation between seismic reflectivity and rheology in extended lithosphere:
1341 Southern Tuscany inner Northern Apennines Italy. *Tectonophysics* 315, 109–122.
1342
1343 Liotta, D., Cernobori, L., Nicolich, R., 1998. Restricted rifting and its coexistence with compressional
1344 structures: results from the Crop03 traverse (Northern Apennines Italy). *Terra Nova* 10, 16–20.
1345
1346 Liotta, D., Brogi, A., Meccheri, M., Dini, A., Bianco, C., Ruggieri, G., 2015. Coexistence of low-angle normal
1347 and high-angle strike- to oblique-slip faults during Late Miocene mineralization in eastern Elba Island
1348 (Italy). *Tectonophysics* 660, 17–34.
1349
1350 Locardi, E., Nicolich, R., 1992. Geodinamica del Tirreno e dell'Appennino centro-meridionale: la nuova
1351 carta della Moho. *Mem. Soc. Geol. Ital.* 41, 121–140.
1352
1353 Losacco, U., 1959. Ricerche geologiche nella Toscana meridionale II. Affioramenti mesozoici della media
1354 Val d'Orcia: Bagno Vignoni, Rocca d'Orcia, Ripa d'Orcia e Pienza (Siena). *Boll. Soc. Geol. It.* 78, 101-
1355 120.
1356
1357 Lister, G.S., Etheridge, M.A., Symonds, P.A., 1986. Detachment faulting and the evolution of passive
1358 continental margins. *Geology*, 14, 246–250.
1359
1360 Ludwig, K.R., 2003. Isoplot/Ex version 3.00, A Geochronological Toolkit for Microsoft Excel. Berkeley
1361 Geochronology Center Special Publication, p. 4.
1362
1363 Luo, L., Wen, H., Li, Y., You, Y., Luo, X., 2019. Mineralogical, crystal morphological, and A.
1364 isotopic characteristics of smooth slope travertine deposits at Reshuitang, Tengchong, China. *Sedimentary
1365 Geology* 381, 29–45.
1366
1367 Mancini, A., Capezzuoli, E., Erthal, M., Swennen, R., 2019. Hierarchical approach to define travertine
1368 depositional systems: 3D conceptual morphological model and possible applications. *Marine and
1369 Petroleum geology*, <https://doi.org/10.1016/j.marpetgeo.2019.02.021>
1370
1371 Mantovani, E., Albarello, D., Tamburelli, C., Babbucci, D., 1995. Evolution of the Tyrrhenian basin and
1372 surrounding regions as a result of the Africa-Eurasia convergence. *J. Geod.* 21, 35–72.
1373
1374 Mantovani, E., Viti, M., Babbucci, D., Tamburelli, C., Cenni, N., Baglione, M., D'Intinosante, V., 2015.
1375 Present Tectonic Setting and Spatio-Temporal Distribution
1376 of Seismicity in the Apennine Belt. *International Journal of Geosciences* 6, 429–454.
1377
1378 Martini, I.P., Sagri, M., 1993. Tectono-sedimentary characteristics and the genesis of the recent
1379 magmatism of Southern Tuscany and Northern Latium. *Per. Mineral.* 56, 157–172.
1380

- 1381
1382
1383 Mazzanti, R., 1966. Geologia della zona di Pomarance-Larderello (Prov. di Pisa). *Mem. Soc. Geol. Ital.* 5,
1384 105–138.
1385
1386 Mazzuoli, R., Tortorici, L., Ventura, G., 1995. Oblique rifting in Salina, Lipari and Vulcano islands (Aeolian
1387 islands, southern Italy). *Terra Nova* 7, 444–452.
1388
1389 Mesci, B.L., Gursoy, H., Tatar, O., 2008. The evolution of travertine masses in the Sivas Area (Central
1390 Turkey) and their relationships to active tectonics. *Turkish Journal of Earth Sciences* 17, 219–240.
1391
1392 Micklethwaite, S., Cox, S., F., 2004. Fault-segment rupture, aftershock-zone fluid flow, and mineralization.
1393 *GSA Geology* 32, 813–816.
1394
1395 Molli, G., 2008. Northern Apennine–Corsica orogenic system: an updated overview. *Geol. Soc. Lond. Spec.*
1396 *Publ.* 298, 413–442.
1397
1398 Muir-Wood, R., 1993. Neohydrotectonics. *Zschr Geomorph Suppl* 94, 275–284.
1399
1400 Negredo, A., M., Barba, S., Carminati, E., Sabadini, R., Giunchi, C., 1999. Contribution of numeric dynamic
1401 modelling to the understanding of the seismotectonic regime of the Northern Apennines.
1402 *Tectonophysics* 315, 15–30.
1403
1404 Pandeli, E., Bertini, G., Castellucci, P., 1991. The tectonic wedges complex of the Larderello area (Southern
1405 Tuscany, Italy). *Boll. Soc. Geol. It.* 110, 621–629.
1406
1407 Panichi, C., Tongiorgi, E., 1976. Carbon isotopic composition of CO₂ from springs, fumaroles, mofettes and
1408 travertines of central and southern Italy: a preliminary prospection method of geothermal area. *Proc.*
1409 *2nd UN Symposium on the Development and Use of Geothermal Energy.* San Francisco, U.S.A., pp.
1410 815–825 Pentecost, A., 2005. *Travertine*, Geologist Association. Springer-Verlag, Berlin, p. 445.
1411
1412 Pascucci, V., Merlini, S., Martini, I., P., 1999. Seismic stratigraphy of the Miocene-Pleistocene
1413 sedimentary basins of the Northern Tyrrhenian Sea and western Tuscany (Italy). *Basin*
1414 *Research*, 11, 337–356.
1415
1416 Pascucci, V., Costantini, A., Martini, I., P., Dringoli, R., 2006. Tectono-sedimentary analysis of a complex,
1417 extensional, Neogene basin formed on thrust-faulted, Northern Apennines hinterland: Radicofani
1418 Basin, Italy. *Sed. Geol.* 183, 81–97.
1419
1420 Pascucci, V., Martini, I.P., Sagri, M., Sandrelli, F., 2007. Effects of transverse structural lineaments on the
1421 Neogene–quaternary basins of Tuscany (inner Northern Apennines, Italy). In: Nichols, G., Williams, E.,
1422 Paola, C. (Eds.), *Sedimentary processes, environments and basins: a tribute to Peter Friend.* Intern. Ass.
1423 *Sediment., Spec. Publ.* 38, 155–182.
1424
1425 Patacca, E., Sartori, R., Scandone, P., 1990. Tyrrhenian basin and Apenninic arcs: kinematic relations since
1426 Late Tortonian times. *Mem. Soc. Geol. Ital.* 45, 425–451.
1427
1428 Pentecost, A., 1994. Formation of laminate travertines at Bagno Vignone, Italy. *Geomicrobiology* , 12, 239-
1429 251.
1430
1431 Pentecost, A., 2005. *Travertine*, Springer, Berlin (445 pp.).
1432
1433 Piccardi, L., Vittori, E., Blumetti, A.M., Quaternary, V. C. 2017. Mapping capable faulting hazard in a
1434 moderate-seismicity, high heat-flow environment: The Tuscia province (southern Tuscany-northern
1435 Latium, Italy). *Quaternary International* 451, 11–36.
1436
1437 Rimondi, V., Costagliola, P., Ruggieri, G., Benvenuti, M., Boschi, C., Brogi, A., Capezzuoli, E., Morelli, G.,
1438 Gasparon, M., Liotta, D., 2015. Investigating fossil hydrothermal systems by means of fluid inclusions

1441
1442 and stable isotopes in banded travertine: an example from Castelnuovo dell'Abate (southern Tuscany,
1443 Italy). *International Journal of Earth Sciences* 105 (22), 659–679.
1444

1445 Rosenbaum, G., Piana Agostinetti, N., 2015. Crustal and upper mantle responses to lithospheric
1446 segmentation in the northern Apennines, *Tectonics*, 34, 648–661.
1447

1448 Rossetti, F., Faccenna, C., Jolivet, L., Funicello, R., Tecce, F., Brunet, C., 1999. Syn-versus post-orogenic
1449 extension: the case study of Giglio Island (Northern Tyrrhenian Sea, Italy). *Tectonophysics* 304, 73–92.
1450

1451 Rossetti, F., Faccenna, G., Jolivet, L., Goffé, B., Funicello, R., 2002. Structural signature and exhumation P–
1452 T–t paths of the blueschist units exposed in the interior of the Northern Apennine chain, tectonic
1453 implications. *Boll. Soc. Geol. It, Spec. Vol. 1*, 829–842.
1454

1455 Rossetti, F., Glodny, J., Theye, T., Maggi, M., 2015. Pressure–temperature–deformation–time of the ductile
1456 Alpine shearing in Corsica: from orogenic construction to collapse. *Lithos* 218–219, 99–116.
1457

1458 Rowland, J.V., Sibson, R.H., 2004. Structural controls on hydrothermal flow in a segmented rift system,
1459 Taupo Volcanic Zone, New Zealand. *Geofluids* 4, 259–283.
1460

1461 Schauer, A.J., Kelson, J., Saenger, C., Huntington, K.W., 2016. Choice of ^{17}O correction affects clumped
1462 isotope ($\Delta 47$) values of CO_2 measured with mass spectrometry. *Rapid Comm. Mass Spec.* 30, 2607–
1463 2616.
1464

1465 Serri, G., Innocenti, F., Manetti, P., 1993. Geochemical and petrological evidence of the subduction of
1466 delaminated Adriatic continental lithosphere in the genesis of the Neogene-Quaternary magmatism of
1467 Central Italy. *Tectonophysics* 223, 117–147.
1468

1469 Shen, C.-C., Cheng, H., Edwards, R.L., Moran, S.B., Edmonds, H.N., Hoff, J.A., Thomas, R.B., 2003.
1470 Measurement of attogram quantities of ^{231}Pa in dissolved and particulate fractions of seawater by
1471 isotope dilution thermal ionization mass spectroscopy. *Anal. Chem.* 75, 1075–1079.
1472

1473 Shen, C.-C., Wu, C.-C., Cheng, H., Edwards, R.L., Hsieh, Y.-T., Gallet, S., Chang, C.-C., Li, T.-Y., Lam, D.D.,
1474 Kano, A., Hori, M., Spötl, C., 2012. High-precision and high resolution carbonate ^{230}Th dating by MC-
1475 ICP-MS with SEM protocols. *Geochim. Cosmochim. Acta* 99, 71–86.
1476

1477 Sibson, R.H., 1987. Earthquake rupturing as a mineralising agent in hydrothermal systems. *Geology* 15,
1478 704–710.
1479

1480 Signorini, R., 1935. Linee tettoniche trasversali nell'Appennino settentrionale, *Rend. R. Accad. Naz. Lincei*,
1481 21, 42–45.
1482

1483 Spötl, C., Vennemann, T.W. 2003. Continuous-flow IRMS analysis of carbonate minerals. *Rapid*
1484 *Communications in Mass Spectrometry*, 17, 1004–1006.
1485

1486 Storti, F., 1995. Tectonics of the Punta Bianca promontory: insights for the evolution of the northern
1487 Apennines–northern Tyrrhenian Sea basin. *Tectonics* 14, 832–847.
1488

1489 Temiz, U., Gökten, E., Eikenberg, J., 2009. U/Th dating of fissure ridge travertines from the Kirsehir region
1490 (central Anatolia, Turkey); structural relations and implications for the neotectonic development of the
1491 Anatolian block. *Geodin. Acta* 22, 201–213.
1492

1493 Te
1494 miz, U., Eikenberg, J., 2011. U/Th dating of the travertine deposited at transfer zone between two normal
1495 faults and their neotectonic significance: Cambazli ridge travertines (the Gediz graben, Turkey).
1496 *Geodin. Acta* 24, 95–105.
1497

1498 Temiz, U., Gökten, Y., E., Eikenberg, J., 2013. Strike-slip deformation and U/Th dating of travertine
1499 deposition: Examples from North Anatolian Fault Zone, Bolu and Yeniçağ Basins, Turkey. *Quaternary*
1500 *International* 312, 132–140.

- 1501
1502
1503 Uysal, I.T., Feng, Y., Zhao, J.X., Altunel, E., Weatherley, D., Karabacak, V., Cengiz, O., Golding, S.D.,
1504 Lawrence, M.G., Collerson, K.D., 2007. U-series dating and geochemical tracing of late Quaternary
1505 travertine in co-seismic fissures. *Earth Planet. Sci. Lett.* 257 (3–4), 450–462.
1506
1507 Uysal, I., T., Feng, Y., Zhao, J.X., Isik, V., Nuriel, P., Golding, S., D., 2009. Hydrothermal CO₂ degassing in
1508 seismically active zones during the late Quaternary. *Chem. Geol.* 265, 442–454.
1509
1510 Vai, G.B., Martini, I.P., 2001. *Anatomy of an Orogen: the Apennines and Adjacent Mediterranean Basins.*
1511 Kluwer Academic Publishers, p. 631.
1512
1513 Vignaroli, G., Berardi, G., Billi, A., Kele, S., Rossetti, F., Soligo, M., Bernasconi, S., M., 2016. Tectonics,
1514 hydrothermalism, and paleoclimaterecorded by Quaternary travetines and their spatio-temporal
1515 distribution in the Albegna basin, central Italy: insights on Tyrrhenian margin neotectonics.
1516 *Lithosphere* 8, 335-358.
1517
1518 Viti, M., Mantovani, E., Babbucci, D., Tamburelli, C., 2006. Quaternary Geodynamics and deformation
1519 pattern in the southern apennines: implications for seismic activity *Boll. Soc. Geol. It* 125, 273-291.
1520
1521 Wedepohl, K., 1995. The composition of the continental crust. *Geochim. Cosmochim. Acta* 59, 1217–1239.
1522
1523 Williams, R.T., Goodwin, L.B., Sharp W.D., Mozley, P.S., 2017. Reading a 400,000-year record of earthquake
1524 frequency for an intraplate fault. *PNAS* 114, 4893-4898.
1525
1526 Zucchi, M., Brogi, A., Liotta, D., Rimondi, V., Ruggieri, V., Montegrossi, G., Caggianelli, A., Dini, A., 2017.
1527 Permeability and hydraulic conductivity of faulted micaschist in the eastern Elba Island exhumed
1528 geothermal system (Tyrrhenian sea, Italy): insights from Cala Stagnone. *Geothermics* 70, 125-145.
1529

1530 **Figure Captions**

- 1531
1532
1533 Fig. 1 - Tectonic sketch of the inner and outer Northern Apennines showing the main structural features:
1534 exhumed HP-metamorphic units, Neogene magmatic bodies, basin-and-range structure with
1535 associated transfer zones in the inner zone; thrusts and developing basins in the outer zone.
1536
1537
1538 Fig. 2 - Geological map of the area indicated in Figure 1, highlighting the main transfer zones associated
1539 to Neogene-Quaternary extensional tectonics, the main thermal springs and gas emission (steam,
1540 CO₂ and H₂S); the Larderello-Travale and Monte Amiata geothermal areas are also highlighted. The
1541 study area, located along the Grosseto-Pienza line, is indicated by the black rectangle, and it is
1542 enlarged in Fig. 3.
1543
1544
1545
1546 Fig. 3 - Geological map of the Bagno Vignoni area and geological sections. Stereographic diagrams
1547 (equal area, lower hemisphere) illustrating faults and striae, kinematic axes and fault plane solutions,
1548 divided per fault-trends and obtained from the inversion of kinematic data collected on fault-slip
1549 surfaces, are also shown.
1550
1551
1552 Fig. 4 - Stratigraphic logs of the tectonic units exposed (and drilled) in the Bagno Vignoni area,
1553 reconstructed through field work and borehole data (Bagno Vignoni 1 borehole in Brogi et al., 2007).
1554 Symbols: O.U.1 - Ophiolite (Middle-Late Jurassic); O.U.2 - sedimentary cover represented by siliceous
1555 limestone, calcarenite, marl with interbedded shale (Calcari a Calpionella and Argille a Palombini
1556 Fms; Early Cretaceous); S.F.1 - Shale, marl, siliceous limestone and radiolarite (Sillano Fm, Early
1557
1558
1559
1560

1561
1562 Cretaceous); S.F.2 - Sandstone, shale and mal (Pietraforte Fm, Cretaceous); S.F.3 - limestone, marl and
1563 shale (Santa Fiora Fm., Cretaceous). S.L.1 - calcarenite, siliceous limestone, shale (Argille e Calcari
1564 Fm; Eocene-Oligocene); T.N.1 - Dolostone and dolomitic limestone (Burano Fm, Late Triass); T.N.2 -
1565 Massive limestone (Calcare Massiccio Fm., Early Lias); T.N.3 - reddish nodular limestone and shale
1566 (Rosso Ammonitico Fm, Middle Lias); T.N.4 - Cherty limestone, marl and shale (Calcare Selcifero Fm.,
1567 Middle-Late Lias); T.N.5 - Marl and marly limestone (Marne a Posidonia Fm, Dogger); T.N.6 -
1568 radiolarite (Diaspri Fm., Malm); T.N.7 - Cherty limestone and marl (Maiolica Fm, Early Cretaceous);
1569 T.N.8 - Shale, marl, radiolarite, siliceous limestone, calcarenite and calcirudite (Scaglia Toscana Fm.,
1570 Late Cretaceous-Late Oligocene); T.N.9 - Quartz-feldspar sandstone, siltstone and shale (Macigno
1571 Fm, Late Oligocene-Early Miocene).

1572
1573
1574
1575
1576 Fig. 5 - Examples of faults and related minor structures; a) a main fault zone affecting the Macigno Fm
1577 along the Orcia River, with offset exceeding 10 m; b) particular of the slip surface and core zone; c)
1578 example of damage zone associated to a meter offset fault affecting sandstone beds belonging to the
1579 Macigno Fm.; d-e) strike-slip faults, associated splay and extensional jogs developed in releasing step-
1580 over zones, representing a minor structure associated with the main transfer zones; f) detail of a
1581 permeable cataclasite, presently cemented by calcite, developed in the core zone of a normal fault; g)
1582 example of superposed kinematic indicators as recognised in rare fault planes; slickensides are made
1583 up of calcite.
1584
1585
1586

1587
1588 Fig. 6 - a) Satellite photograph (from Google Earth) illustrating the Bagno Vignoni travertine deposits
1589 and the main faults as reconstructed through the field work (see also Fig. 3). Fissure ridge-type
1590 travertine deposits (A, B and C correspond to fissure ridges described in the text), thermal springs
1591 and the abandoned quarries are also reported; b-c) panoramic views of the active travertine slope-
1592 depositional system occurring nearby the SPA; d) main thermal spring feeding the Medieval pool and
1593 giving rise to the travertine deposition.
1594
1595

1596
1597 Fig. 7 - Morphometric analyses and photographs of the fissure ridges A and B (see Fig. 6 and 10 for their
1598 location).
1599

1600
1601 Fig. 8 - Photographs of the saw-cut wall illustrating the inner part of the fissure ridge C (see Fig. 6 and
1602 10 for its location); a-b) saw-cut wall of the quarry and the line-drawing with the interpretation of the
1603 geometrical setting and progressive development; c-d) particular of the angular unconformity and
1604 banded calcite vein characterising the travertine body.
1605

1606
1607 Fig. 9 - a) Panoramic view of the Quarry 3 where the high- and low-energy travertine depositional
1608 environments are highlighted; see the text for more information on the facies distribution and
1609 travertine features. b) detail of the lithofacies 2 (as described in the text) typical of running waters
1610 along slopes; c) detail of the lithofacies 1 and 4 (as described in the text) developed in low-energy
1611 (palustrine) environment; d) example of reed association characterising a travertine level deposited in
1612 a palustrine environment; e) detail of the blocks characterising the lithofacies 3 and delimited, at the
1613 top, by an erosional surface.
1614
1615
1616
1617
1618
1619
1620

1621
1622 Fig. 10 - a) Sketch-map of a part of the western travertine deposit (see Fig. 6 for its location) where the
1623 abandoned quarries are located. The twelve Stratigraphic Units (S.U.0-11) that have been recognised
1624 through the analyses of the quarries saw-cut walls are indicated with different colours. In addition,
1625 the location of the banded calcite veins, palaeothermal springs forming mounds and fissure ridges are
1626 also reported. b) panoramic view of the northern wall of the Quarry 2, where the S.U0-S.U5 have been
1627 described; c-d) panoramic view of the northern wall of the Quarry 3, where the S.U2-S.U7 have been
1628 described; e) panoramic view of the eastern wall of the Quarry 23, where the S.U7-S.U8 forming the
1629 western slope of the fissure ridge B are exposed.
1630
1631

1632
1633 Fig. 11 - Particular of fault zones filled by banded calcite veins exposed in the eastern saw-cut wall of the
1634 Quarry 2 (see Fig. 10 for location); a) panoramic view of the fault zones and banded calcite veins.
1635 Note how the fault zone 1 affected only the S.U0; it was and unconformably overlaid by the S.U1; on
1636 the contrary, fault zone 2 dissected both S.U0 and S.U1. b) particular of the fault zone 2 highlighting a
1637 fracture affecting the bedded travertine, filled by bedded travertine lithons travertine and dissected
1638 again during a hydrothermal fluids circulation that deposited the banded calcite vein; c-f) particular
1639 of the banded calcite veins filling the fault zones; e) fractures filled by calcite and paleosoil affecting
1640 the bedded travertine of the S.U0. Ages are also reported and indicated in Table 3.
1641
1642
1643
1644

1645 Fig. 12 - a-c) Particular of the saw-cut wall of the Quarry 3 (Fig. 10 for the location) showing a banded
1646 calcite vein crossing the travertine deposit and its substratum, made up of Late Eocene calcarenite
1647 belonging to the Scaglia Toscana Fm. d-e) example of banded calcite veins crossing the banded
1648 travertine outside of the quarries. Ages are also reported and indicated in Table 3.
1649
1650

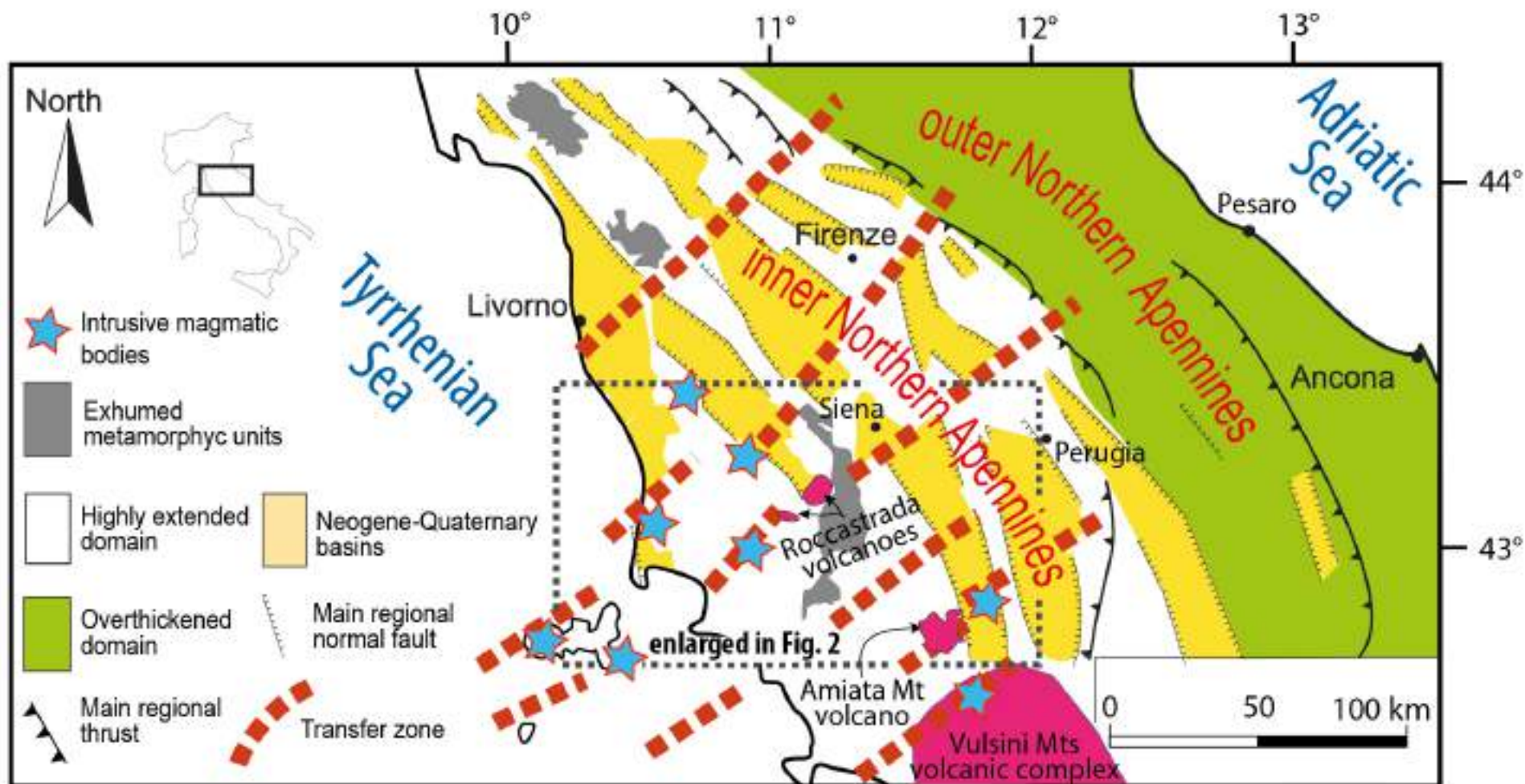
1651 Fig. 13 - Example of the texture of the banded calcite vein: a) banded calcite vein and thin section across
1652 the whole vein in the indicated area; b) thin section (polarized light) showing the fabric of the calcite
1653 crystals forming the different bands of the vein; see the text for more information.
1654
1655

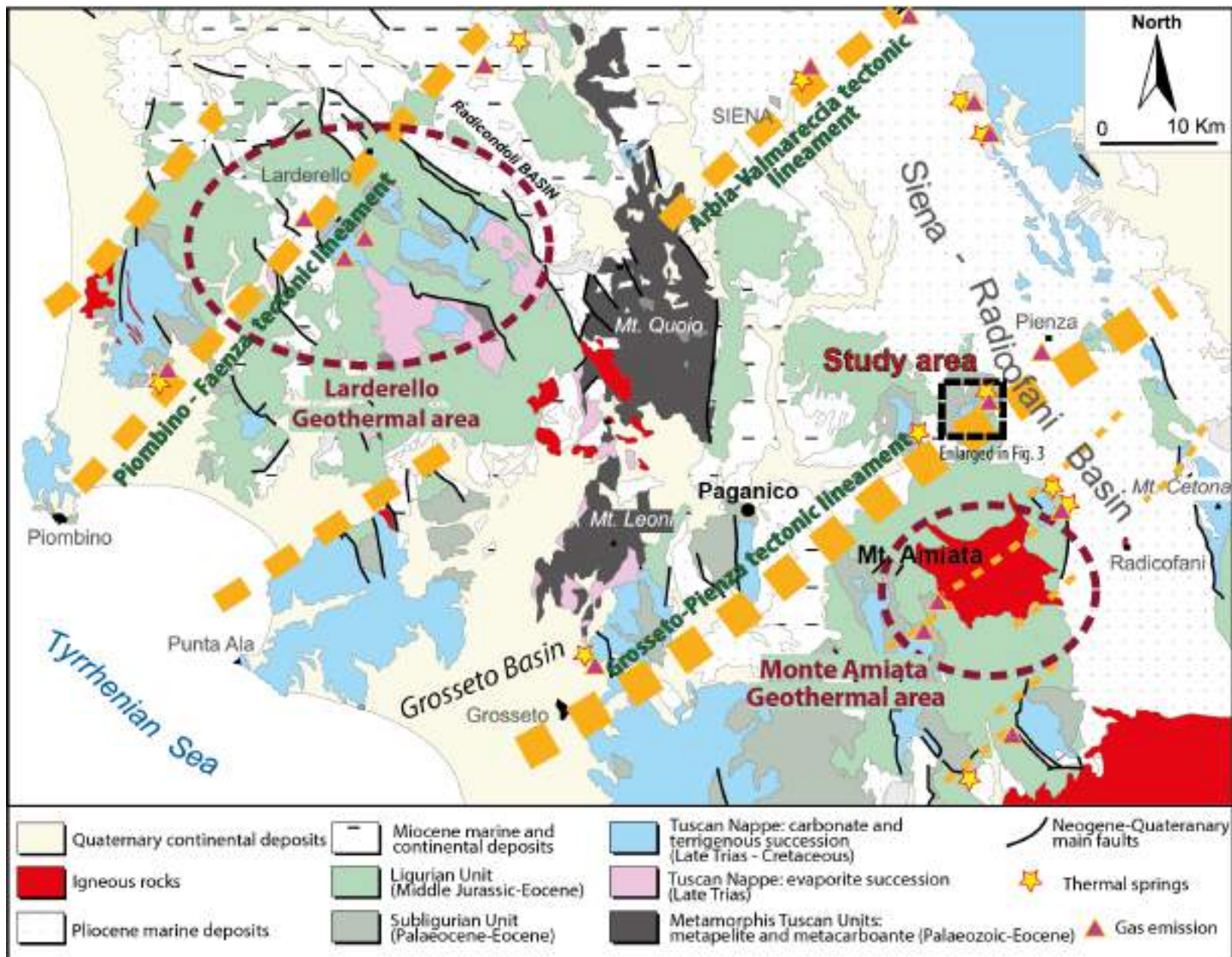
1656 Fig. 14 - Isotope values of the studied samples compared with samples from other areas characterised by
1657 similar settings (see the text for more information); data from Bagni S. Filippo, Le Zitelle and Terme
1658 San Giovanni are from Gandin and Capezzuoli (2008); data from Sarteano are from (Rimondi et al.,
1659 2016).
1660
1661

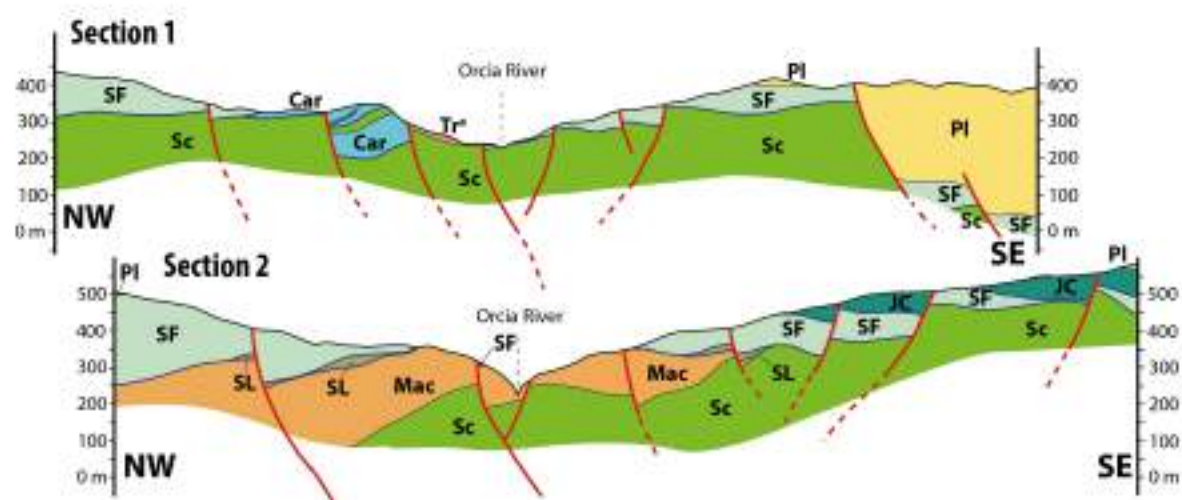
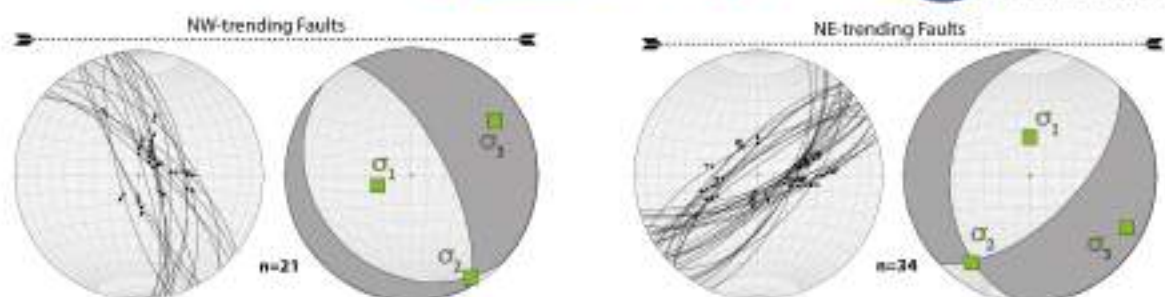
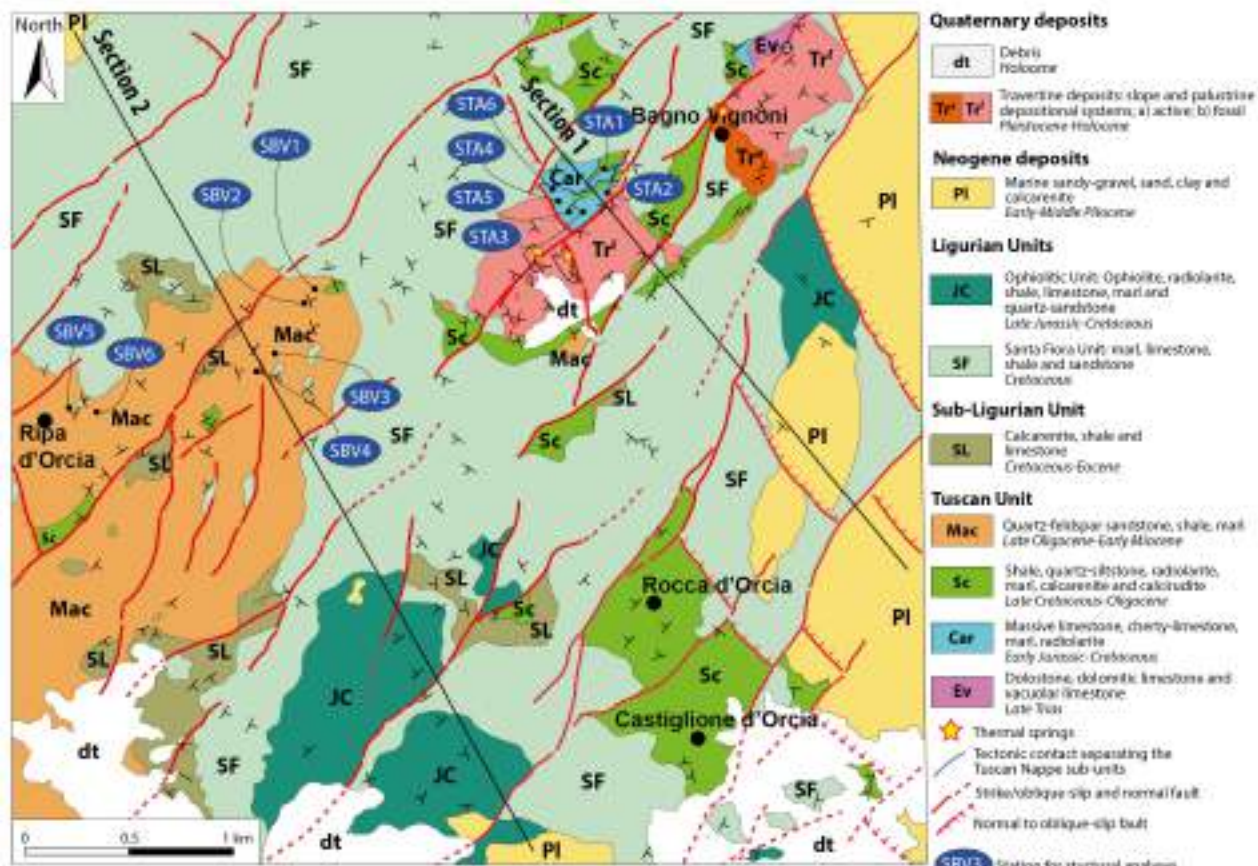
1662 Tab. 1 - List and characteristics of analysed samples. Their location is indicated in Fig. 10a.
1663
1664

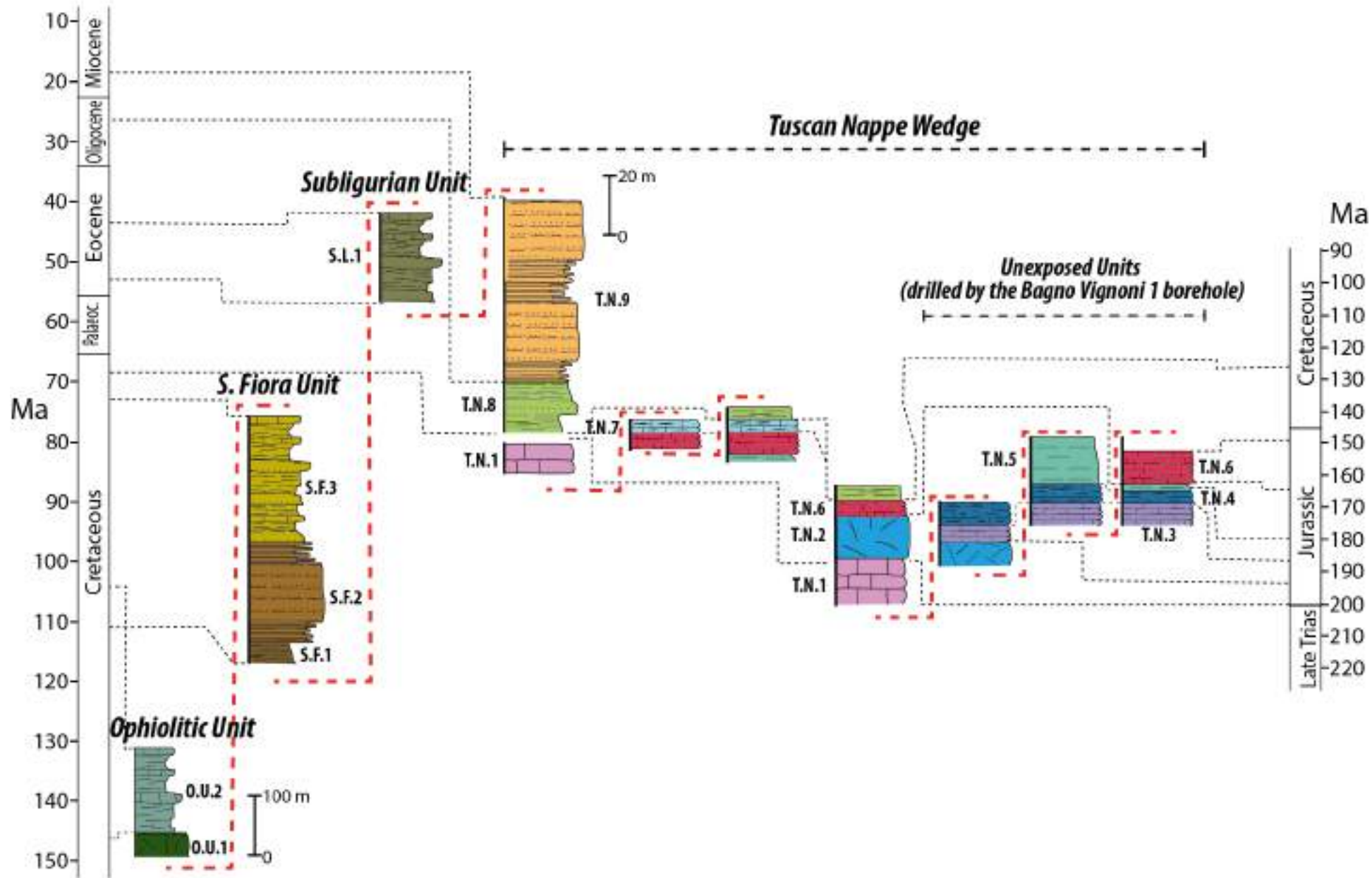
1665 Tab. 2 - Results of the stable and clumped isotopes analyses
1666
1667

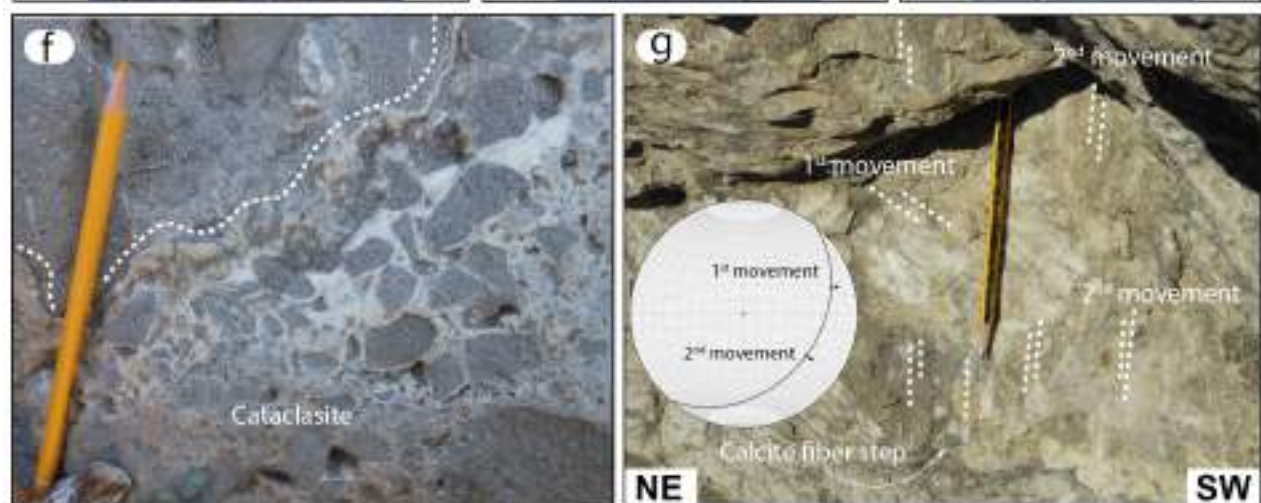
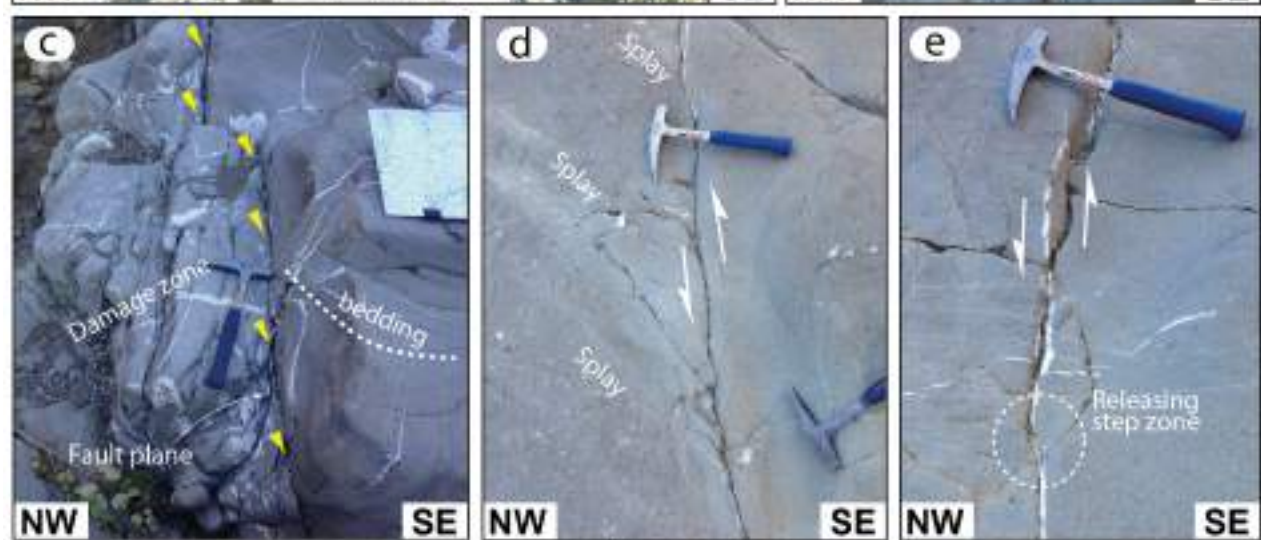
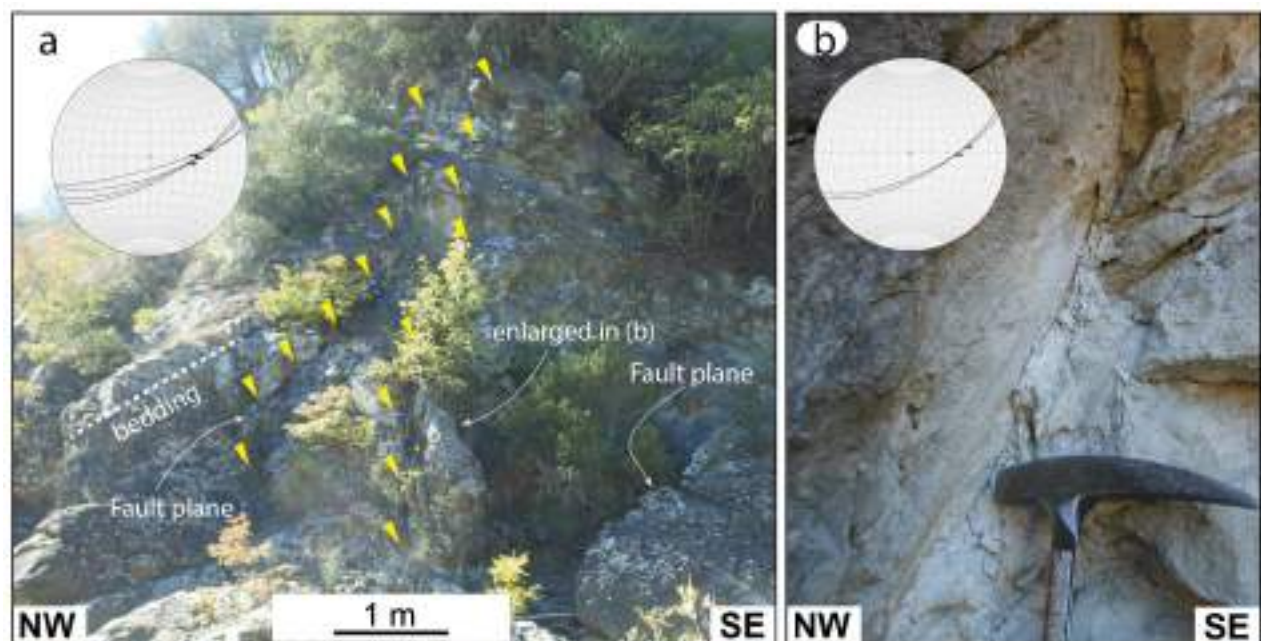
1668 Tab. 3 - Uranium isotopic composition and U-Th ages for travertines of Bagni Vignoni.
1669
1670
1671
1672
1673
1674
1675
1676
1677
1678
1679
1680

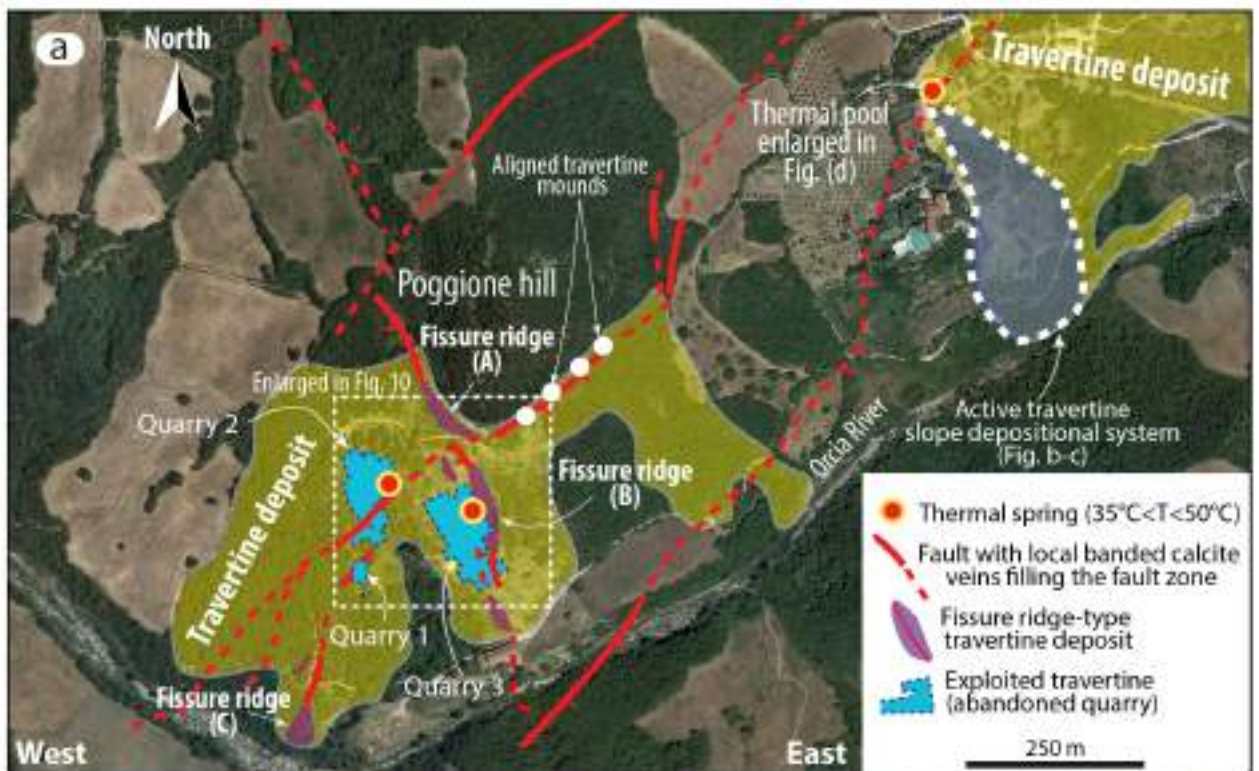




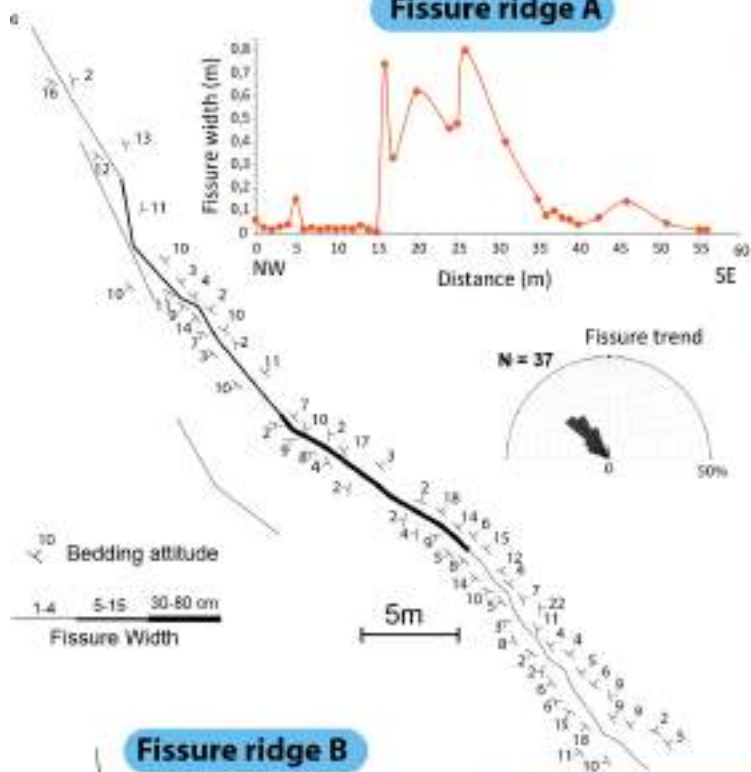








Fissure ridge A



Fissure ridge B

